Coordination Chemistry Reviews 255 (2011) 804–824

Contents lists available at ScienceDirect

Coordination Chemistry Reviews

journal homepage: www.elsevier.com/locate/ccr

Review

Electron transfer reactions of rigid, cofacially compressed, π-stacked porphyrin–bridge–quinone systems

Youn K. Kang[a,1], Peter M. Iovine[b], Michael J. Therien[c,*]

[a] Division of Chemistry and Molecular Engineering, Department of Chemistry, College of Natural Sciences, Seoul National University, Seoul 151-747, Republic of Korea
[b] Department of Chemistry & Biochemistry, University of San Diego, San Diego, CA 92110, USA
[c] Department of Chemistry, French Family Science Center, 124 Science Drive, Duke University, Durham, NC 27708, USA

Contents

ARTICLE INFO

Article history:
Received 12 October 2010
Accepted 10 December 2010
Available online 6 January 2011

Keywords:
Electron transfer
Cofacial porphyrin quinone
Transient dynamics
Synthesis

ABSTRACT

A 1,8-naphthyl pillaring motif can be utilized to enforce sub van der Waals interplanar separations between juxtaposed porphyryl, aromatic bridge, and quinonyl components of donor–spacer–acceptor (D–Sp–A) compounds. Such structures, synthesized via metal-mediated cross-coupling of appropriately functionalized (porphinato)zinc(II), arene, and quinone precursors, manifest unusual conformational rigidity in the condensed phase, and significant electronic communication between the cofacially aligned D, Sp, and A components. NMR experiments provide rigorous determination of the ambient temperature structures of these species in solution, while computational methods offer insight into the fragment molecular orbital interactions that give rise to the strong D–A coupling evident in these assemblies. The distance-, temperature-, and solvent-dependences of photoinduced charge separation (CS) and thermal

* Corresponding author. Tel.: +1 919 660 1670; fax: +1 919 684 1522.
E-mail address: michael.therien@duke.edu (M.J. Therien).
[1] Current address: Department of Chemistry, Sangmyung University, Seoul 110-743, Republic of Korea.

0010-8545/$ – see front matter © 2011 Elsevier B.V. All rights reserved.
doi:10.1016/j.ccr.2010.12.011

charge recombination (CR) rate constants in these systems have been evaluated using femtosecond visible pump/vis–NIR probe and visible pump/mid-IR probe transient dynamical methods. These experiments: (i) demonstrate that simple aromatic building blocks like benzene, which are characterized by highly stabilized filled molecular orbitals and large HOMO–LUMO gaps, provide substantial D–A electronic coupling when organized within a π-stacked structural motif that features a modest degree of arene–arene interplanar compression; (ii) assess directly the degree of ground and excited state charge transfer (CT) in these donor–spacer–acceptor (D–Sp–A) structures, (iii) reveal unusual CS dynamics from vibrationally relaxed and unrelaxed S_1 states, and (iv) show a photoinduced CS mechanistic transition from the nonadiabatic to the solvent-controlled adiabatic regime, to one where CS becomes decoupled from solvent dynamics and is determined by the extent to which the vibrationally unrelaxed S_1 state is populated.

1. Introduction

A plethora of molecular structures have been used to probe mechanically photoinduced electron transfer (ET) reactions relevant to early photosynthetic charge separation events [1–51]. Factors that include the nature of reaction energetics, the magnitudes of inner- and outer-sphere nuclear reorganization energies, and the extent of electronic coupling between the reactant and the product states play important roles in such reactions [52–60]. An extensive body of experimental and theoretical data developed over several decades provides a roadmap that enables facile manipulation of the magnitudes of ET rate constants for many donor–acceptor (D–A) architectures.

The magnitude of the D–A electronic coupling is sensitive to the electronic structure of the D and A, the molecular bridge or spacer (Sp) that connects these species, the modes of D–Sp and Sp–A connectivity, geometric factors, and the energy gaps that separate the relevant D, Sp, and A frontier orbitals. Many of nature's charge transfer reactions occur over large D–A distances; as such, there has been significant interest in ET media and Sp structures that support significant electronic coupling over long D–A distances. Pioneering theoretical work recognized that electronic coupling for long-range ET reactions often involved super-exchange via off-resonance coupling to the medium (or Sp) virtual electronic states [61–64], in contrast to direct D–A exchange. In this manuscript, we review our studies of electronic coupling and charge transfer dynamics in a strongly electronically coupled D–Sp–A system that possesses unusual modes of D–Sp and Sp–A connectivity; these assemblies feature a 1,8-naphthyl pillaring motif that enforces sub van der Waals interplanar separations between juxtaposed, π-stacked porphyryl, aromatic bridge, and quinonyl components.

The theoretical framework that describes nonadiabatic (weak D–A electronic coupling limit) electron transfer was developed largely by Marcus (Eq. (1)) [53,54],

$$k_{ET} = \frac{2\pi}{\hbar}\frac{H_{DA}^2}{\sqrt{4\pi\lambda_T k_B T}}\exp\left(-\frac{(\Delta G+\lambda_T)^2}{4\lambda_T k_B T}\right) \quad (1)$$

where k_B and $\hbar$ are the respective Boltzmann and Planck constants, H_{DA} is the electronic coupling matrix element, T is the temperature, ΔG is the free energy difference between the reactant and product states, and λ_T is the total reorganization energy which is the sum of an inner sphere term, λ_i, and an outer sphere term, λ_o (Eq. (2)) [53–55].

$$\lambda_T = \lambda_i + \lambda_o \quad (2)$$

This ET rate expression can be extended to account for quantum mechanical effects; a simple version of such an expression considers the case where a singly averaged high-frequency, intramolecular vibrational mode is coupled to the ET event. Here, a single reactant state free energy surface couples to multiple high-frequency vibrational modes of the product state (Eqs. (3) and (4)) [57–60].

$$k_{ET} = \frac{2\pi}{\hbar}\frac{H_{DA}^2}{\sqrt{4\pi\lambda_{cl}k_B T}}\exp(-S_c)\sum_{m=0}^{\infty}\frac{S_c^m}{m!}\exp\left(-\frac{(\Delta G+\lambda_{cl}+m\hbar\langle\omega\rangle)^2}{4\lambda_{cl}k_B T}\right) \quad (3)$$

$$S_c = \frac{\lambda_i}{\hbar\langle\omega\rangle} \quad (4)$$

In these expressions, $\langle\omega\rangle$ is the average frequency of the high-frequency vibrational modes in the reactant state, S_c is the Huang–Rhys factor [65] that expresses the extent of nuclear coupling, which can be approximately described in terms of the displacement of the intramolecular equilibrium nuclear configuration accompanying ET [66]. λ_i is the nuclear reorganization energy related to the quantum mechanical, high-frequency intramolecular vibrational modes that are coupled to the ET reaction, λ_{cl} is the reorganization energy of classical modes that include solvent polarization and low-frequency intramolecular vibration, and m is the high-frequency vibrational quantum number. Other parameters are the same as those described for Eq. (1). Eq. (3) can be recast in the form

$$k_{ET} = \frac{2\pi}{\hbar}H_{DA}^2 F \quad (5)$$

where F is the Franck–Condon (FC) factor, which represents the sum of the products of the overlap integrals of the vibrational and solvational wavefunctions of the reactant with those of the products, that are appropriately Boltzmann factor weighted [67]. The squared electronic coupling matrix element is expected to decrease approximately exponentially with distance (Eq. (6)); the nature of this exponential decay is expressed by the decay parameter β^H, which is sensitive to the electronic nature of the D, A, and Sp (tunneling medium).

$$\left|H_{DA}\right|^2 = \left|H_0\right|^2\exp[-\beta^H(R_{DA}-R_0)] \quad (6)$$

In Eq. (6), R_{DA} is the D–A separation distance, R_0 is the smallest possible D–A separation distance (~3.0), H_{DA} is the electronic coupling at R_{DA}, and H_0 is the electronic coupling at R_0. Importantly, not only H but also F may affect the distance dependence of the observed ET rate constant, through the distance dependence of the reaction free energy and the reorganization energy, which cannot be expressed in general mathematical form [68]. This combined effect gives rise to an expression characterizing the phenomenological distance dependence of the ET rate constant; note that the parameter β in Eq. (7) generally differs from β^H.

$$k_{ET} = k_0\exp[-\beta(R_{DA}-R_0)] \quad (7)$$

A large body of work has probed how the nature of the tunneling medium impacts the magnitude of the ET rate constant; exemplary Sp structures that have been extensively investigated in this regard include nonconjugated and conjugated covalent bonds, peptides, proteins, DNA, and H-bonded structures [5,46,59,69–215]. In the late 1980s, Barton pioneered the use of double-stranded DNA as a template to interrogate electronic

coupling through stacked, π-cofacial assemblies [91–111]. Giese [192–197], Lewis and Wasielewski [180–187], Schuster [172–176], Meade [177–179], Beratan [124–126,129], Tanaka [189,190] and Fukui [189–191], and Ratner [165,216–220] have since investigated a wide range of mechanistic issues related to DNA-mediated charge transport.

ET assemblies that utilize double-stranded DNA as the Sp separating D from A define model assemblies with which to probe electronic coupling mediated by π-cofacial aromatic units. In DNA, the average nucleobase–nucleobase interplanar separation is about 3.5 Å, and experimental studies of the distance-dependent kinetics have produced a wide range of results. Like double-helical DNA constructs that mediate charge transfer reactions, conventional synthetic π-stacked structures provide little insight into how the magnitude of the interplanar separation distance might impact electronic coupling in π-cofacial assemblies. In this article, we summarize our studies of a unique, rigid class of D–Sp–A structures in which sub-van der Waals interplanar distances separate the juxtaposed D, Sp, and A units in a π-stacked configuration, and discuss: (i) the synthesis and structural characterization of these systems, (ii) their photoinduced charge separation (CS) and thermal charge recombination (CR) dynamics, and (iii) the nature of electronic coupling manifest in these constructs.

2. Synthesis and structural characterization of cofacially compressed, π-stacked porphyrin–bridge–quinone systems

Molecular architectures that feature π-stacked aromatic manifolds have attracted a great deal of interest in fields of physical organic chemistry, materials chemistry, and catalysis, yet they remain challenging synthetic targets [221]. One of the greatest challenges in this area is identifying molecular scaffolds that are synthetically accessible, yet capable of orienting and fixing the position of aromatic moieties in a stacked columnar arrangement. Such well-defined assemblies are unusual, yet such systems provide the ability to predictably control the nature of electronic interactions within the aromatic stack, enabling delineation of important structure–property relationships. We thus note briefly below benchmark examples of precise π-stacked architectures, before moving on to a more detailed review of our work.

The [*n.n*]paracyclophanes define the quintessential π-stacked architecture [222–233]. In cases where the methylene bridges are short (3–4 carbons), the paracylophane's arene units experience restricted rotation and are forced to adopt a stacked arrangement. These π-stacked systems have been extensively examined in relation to the degree of intramolecular charge transfer as a function of arene conformation. Likewise, Rathore has extensively examined π-stacked polyfluorenes [215,234,235]. In these systems, fluorene rings are held in a cofacial arrangement by a saturated aliphatic backbone. Using both X-ray crystallographic methods and NMR spectroscopy, it was determined that the fluorene rings are held in van der Waals contact and maintain their cofacial arrangement in both solution and the solid state. Waldeck and Paddon-Row have examined electronic coupling through rigid cofacially oriented structures that are separated by distances that significantly exceed those defined by van der Waals radii [236–239]. In contrast, Lewis developed oligo(arylureas) – a covalently linked, more loosely π-stacked architecture that adopts a folded protophane structure [240,241]. In these assemblies, arylurea rings fold into face-to-face geometries featuring slightly spayed phenyl rings. The end groups of these oligomers can easily be modified with D–A groups that facilitate the study of intramolecular charge transfer. It was found that rate constants for CS and CR in these assemblies were weakly dependent upon the number of bridging units.

As underscored by the extensive literature in the area [91–111,124–126,129,165,172–187,189–197], the popularity of double-stranded DNA and related nucleobase scaffolds for interrogating issues pertinent to stacked π manifold electronic coupling derives largely from their ease of synthesis. Fabrication of π-stacked assemblies, in which interactions between cofacially aligned D, Sp, and A moieties differ radically from deoxyribonucleic acid-based systems, is inherently more challenging. Even so, the fact that so few such assemblies exist is perhaps surprising, given the potential impact that both the magnitude of respective D, Sp, and A interplanar separations, and the nature of the quadrupolar interactions between these aromatics may have upon the regulation of electronic coupling [242–244]. In 2000, we first reported the synthesis and characterization of unusually rigid, cofacially aligned, porphyrin–bridge–quinone systems featuring compressed π manifolds (Fig. 1) [245]. We later expanded the collection of these D–Sp–A molecules (Fig. 1) [149], and showed that the modular design of these π-stacked systems allows for a systematic investigation of the distance dependence of D–A coupling in π stacked manifolds in which the juxtaposed planar units are separated by distances less than that of van der Waals contact (3.40 Å), and thus sharply contrast the helix rise per base pair distance found in B-DNA. The separation between adjacent, cofacially-aligned aromatic moieties in these assemblies is fixed by the 1,8-substitution pattern of naphthalene, which serves as the pillar that links D, Sp, and A. The substantial geometric constraints imposed by the 1,8-naphthalene skeleton make this unit an ideal scaffold to build rigid, stacked π manifolds.

The synthetic challenge of covalently linking multiple (>2) arene units in a closely held cofacial π-stacked arrangement is formidable; few molecular scaffolds have possible utility in this regard, which is underscored by the fact that traditional routes to cyclophanic architectures make difficult the design and synthesis of such systems. While cyclophanic systems can in fact enforce a sub-van der Waals interplanar separation between juxtaposed arenes, systematic modulation of the electronic structure of the components of these assemblies, as well as the expansion of this motif to multiple levels of π-stacking interactions, define arduous synthetic tasks. Due to the modular nature of the route exploited in the fabrication of π-stacked compounds **1**, **2a**–**c**, and **3a**, structure–function relationships that determine the magnitude of D–A electronic coupling were more readily probed.

Scheme 1 highlights some of the reagents, coupling protocols, and reaction conditions that were employed in the syntheses of compounds **1**–**3**. Modified Suzuki conditions, developed for systems in which hydrolytic deboronation is a significant side reaction, were required for many of the coupling reactions. This cross-coupling protocol is carried out under anhydrous conditions, employing a dry polar solvent (DMF) and weakly soluble base (K_3PO_4); all carbon–carbon bond forming reactions involving the 1-iodo-8-arylnaphthalenic substrate were carried out under these conditions, which effectively suppressed deleterious dehalogenation and deboronation processes.

The conversion of the 2,5-dimethoxyphenyl groups to their corresponding quinoidal derivatives was accomplished using a Lewis acid-promoted demethylation followed by a mild oxidation of the newly formed hydroquinone [245]. In contrast, this simple deprotection–oxidation sequence proved ineffective for the generation of compound **1a-Zn** due possibly to the close proximity of the 2,5-dimethoxyphenyl ring to the porphyrin macrocycle. In this particular case, more forcing conditions were required to fully convert the dimethoxyphenyl group to its corresponding quinone.

In advance of studying the electron transfer processes in these compressed π-stacked systems, we undertook a comprehensive study aimed at delineating the solution structural dynamics [246]. With such information, key structure–function and

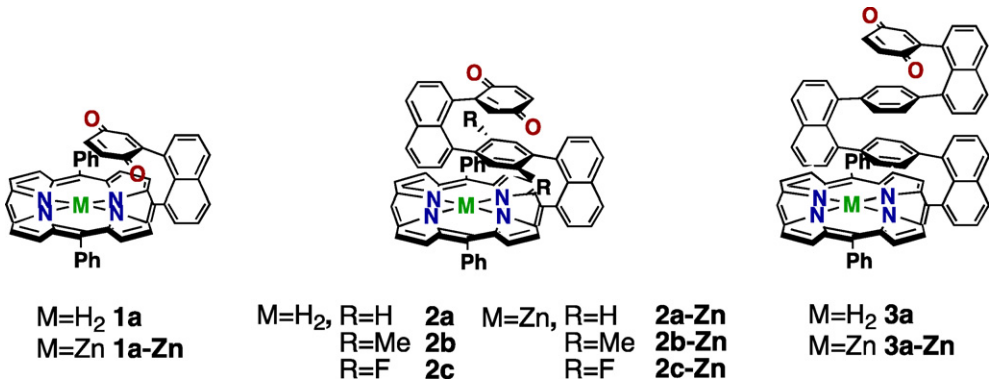

Fig. 1. Chemical structures of porphyrin–bridge–quinone compounds used to study electron transfer dynamics in π-stacked architectures.

structure–property relationships can be ascertained independent of the assumption that the liquid-phase structure is identical to that determined for the solid state by X-ray crystallographic methods.

The rigid geometry coupled with the sub-van der Waals interplanar separations manifest in these porphyrin-based D–Sp–A systems gives rise to disparate shielding effects which distribute the aromatic ^{1}H resonances for these species over wide spectral windows. The favorable structural and spectroscopic properties of these newly defined π-stacked D–Sp–A assemblies allowed the acquisition of a substantial number of structurally significant NOEs which define key interplanar relationships between the porphyrin, phenyl spacer, and benzoquinonyl units; these data were incorporated as restraining functions in *ab initio* simulated annealing (SA) calculations, enabling a high-resolution solution structure of **2a** to be determined.

Complete and unambiguous assignment of the ^{1}H NMR resonances for **2a** was accomplished using 1D ^{1}H NMR, 2D homonuclear COSY, and 2D NOESY NMR experiments. The 1D ^{1}H NMR spectrum of compound **2a** manifests the following spectral features: (i) distribution of aromatic resonances over a spectral window that spans 10.20–0.62 ppm, (ii) groupings of signals that derive from disparate shielding effects as a result of an upright, π-stacked geometry, and (iii) sharp resonances which exhibit little-to-no spectral overlap. Fig. 2 divides the spectrum into two regions labeled A and B. Region A contains those resonances ascribed to the porphyrin β pyrrolic protons, the porphyrin 10,20-phenyl substituents, as well as the protons residing on the Naphthalene I pillar (Fig. 2). Region B contains the resonances associated with the Naphthalene II pillar, the intervening phenyl spacer (H_1–H_4, Fig. 2), and the protons residing on the quinonyl subunit.

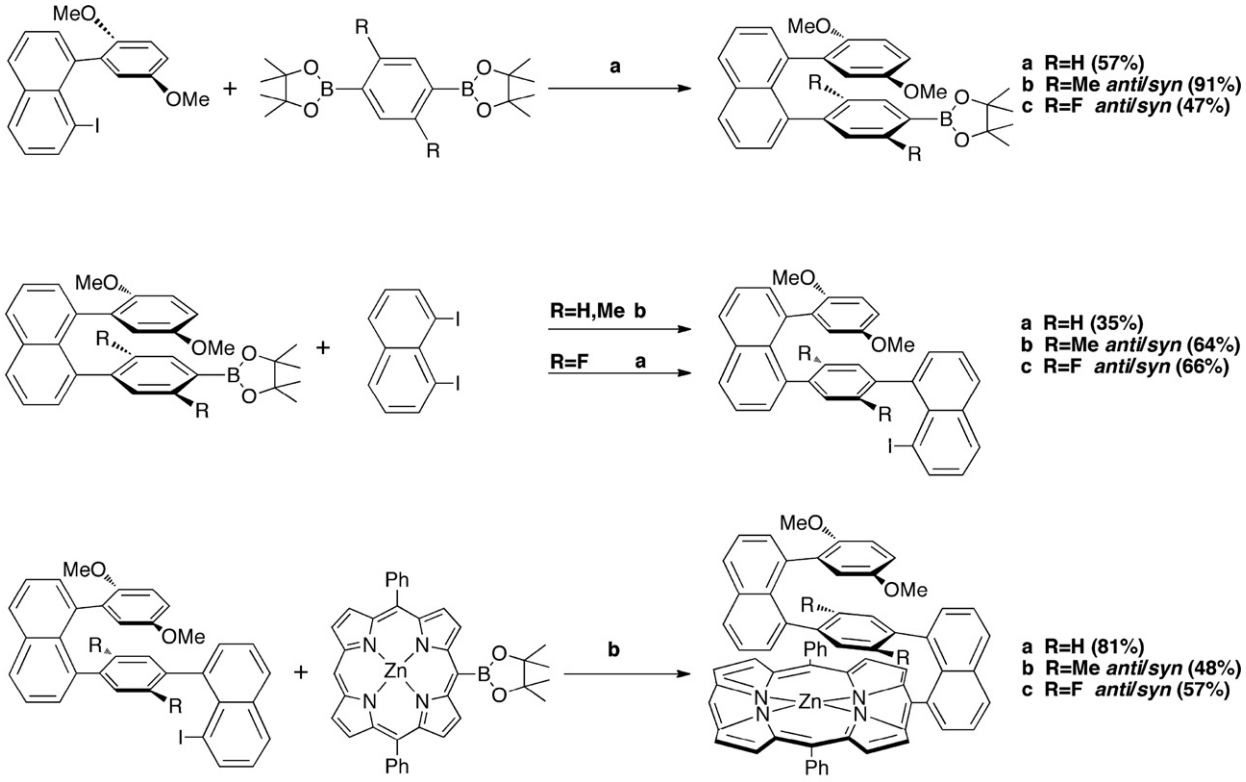

[a] Key: (a) K_3PO_4, $Pd(Ph_3)_4$, DMF, 100 °C; (b) $Ba(OH)_2{\cdot}8H_2O$, $Pd(Ph_3)_4$, DME/H_2O, 80 °C.

Scheme 1. Sequential Suzuki–Miyaura coupling reactions were used to synthesize a series of unusually rigid π-stacked porphyrinic assemblies featuring a cofacially aligned π manifold.

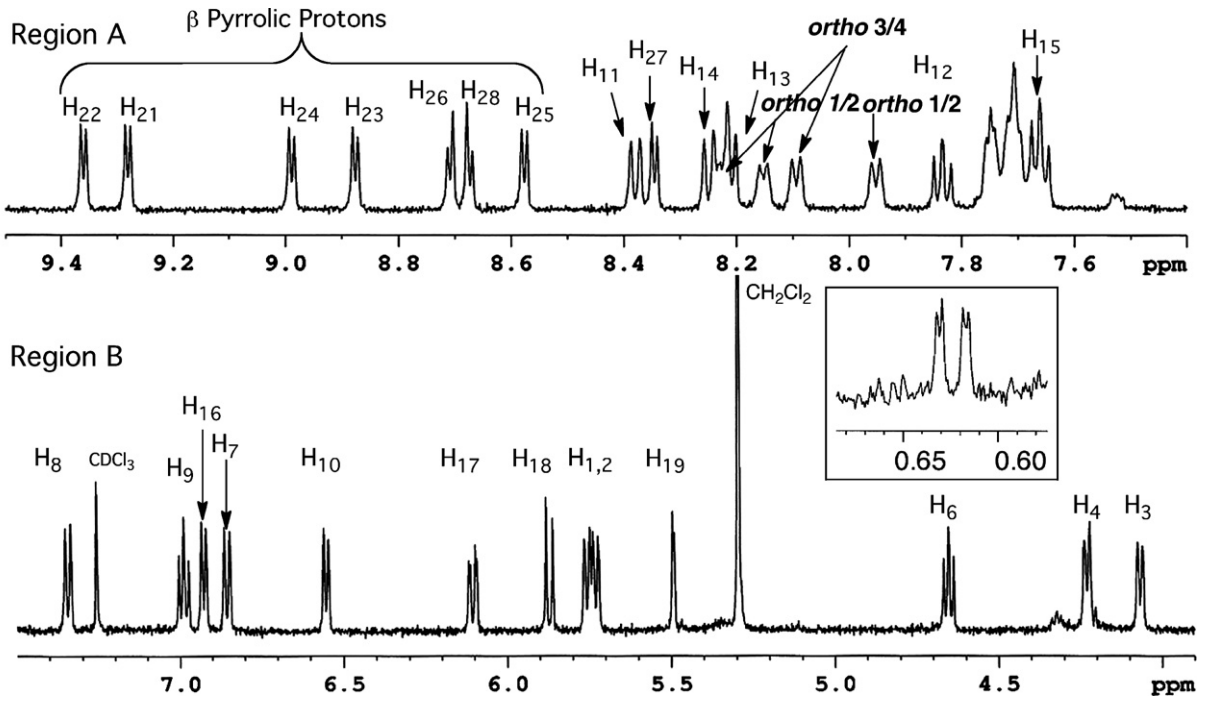

Fig. 2. 500 MHz ^{1}H NMR spectrum of 5-[8′-(4″-[8‴-(2⁗,5⁗′-benzoquinonyl)-1‴-naphthyl]-1″-phenyl)-1′-naphthyl]-10,20-diphenylporphyrin (**2a**) in $CDCl_3$ highlighting the distribution of aromatic resonances over a large spectral window (10.20–0.62 ppm) due to the disparate shielding effects of the π-stacked geometry [246].

A set of 11 interproton distances (Fig. 3) which define key structural relationships in **2a** were extracted from the NOESY spectrum; these NOESY-derived constraints were used as restraining functions in the MD/SA calculations for compound **2a**. The 50 lowest energy structures generated using the MD/SA analysis were further refined using CHARMm-based energy minimization; these studies determined the distribution of energies among the conformers and evaluated the extent to which the calculated structures were consistent with the empirical NOESY data.

The 50 refined structures were evaluated for NOE violations in excess of 0.5 Å, which represents the limit of confidence for the NMR measurements; all 50 structures satisfied this conformational restraint. Remarkably, when more stringent criteria were used (i.e., a 0.2 Å NOE violation limit), 41 of these 50 computed minimum energy structures were finally accepted. An average structure was calculated from the 50 refined conformers that considered **2a**'s entire 52 carbon atom framework. The root-mean square deviation (RMSD) of the 50 conformers with respect to the consensus structure was calculated to be 0.51 Å.

The 50 energy-minimized conformers derived from *ab initio* SA calculations were used as initial structures for restrained minimization in CHARMm. NOE violations of 0.5 Å were found in only 2 of the 50 structures; lowering the acceptance threshold for the NOE violations to 0.2 Å excluded only 4 of the 50 structures, an improvement from the 9 structures found to have violations in the *ab initio* SA analysis. Structural representations of the low energy structure are shown in Fig. 4 (van der Waals spheres at 80%).

Several features of the calculated structure deserve comment. A labeling schematic for the critical distances and angles used is shown in Fig. 3; the corresponding numerical data can be found in Table 1 (Fig. 5).

One of the most striking features of the calculated structure is the closely packed, π-stacked arrangement of the porphyrin donor, intervening phenyl spacer, and the quinone acceptor. For example, the internuclear distance separating the C1 and C1′ carbon atoms (distances A and B, Fig. 5) of the 1-quinonyl and 1-phenyl substituents of Naphthalene II is 2.97 Å and 0.4 Å below the van der Waals separation distance; these data are consistent with X-ray crystallographic data for the analogous distance separating the C1′ and C1″ carbon atoms in 1,8-diphenylnaphthalene (2.99 Å, Table 1; distance A, Fig. 5). Similarly, a sub van der Waals separation (2.97 Å) is also observed for the distance labeled D in Fig. 5b. Note also that the A and C distances in the calculated structure are consistent, suggesting that the hallmark sub van der Waals separation associated with simple 1,8-diarylnaphthalenes is maintained despite the incorporation of a large porphyrinic substituent at the Naphthalene I's 1-position.

Perhaps the most remarkable aspect of the 1D ^{1}H NMR spectrum of **2a** is the chemical shift determined for aromatic proton H_5

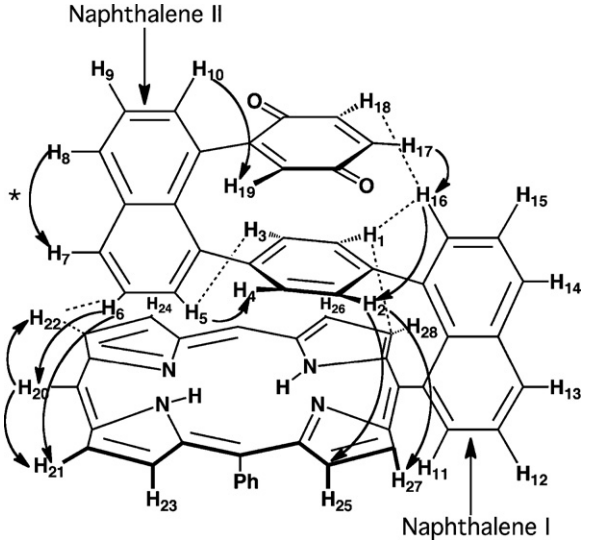

Fig. 3. Schematic illustrating the large number of NOE signals identified in compound **2a**. The compressed geometry of the **2a**'s porphyrinic assembly positions multiple aromatic residues in close proximity and leads to wealth of structural information that can be used to calculate a NMR-based solution structure [246].

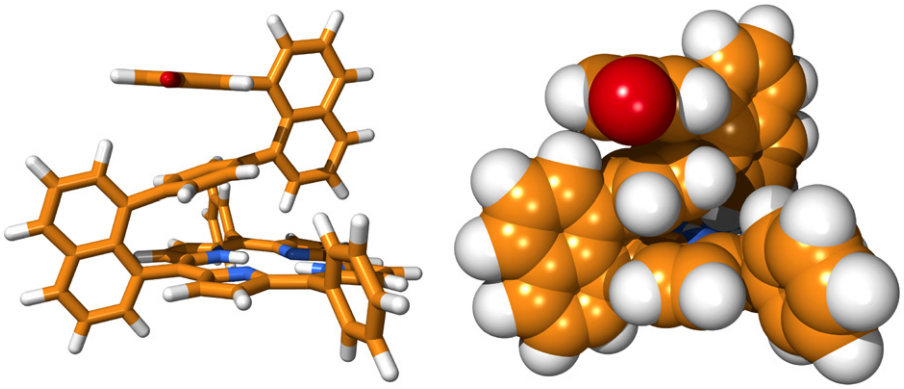

Fig. 4. Low energy structure of **2a** with van der Waals spheres at 80% [246].

Table 1
Comparative distances separating π-stacked ring systems in the low energy structure **2-H$_2$** (determined from *ab initio* SA analysis incorporating NOESY restraints and subsequent CHARMm restrained minimization) and 1,8-diphenylnaphthalene.[a]

Label	Calculated distance (Å)	
	2a$_{low}$[b]	1,8-Diphenylnaphthalene[c]
A	2.97	2.99
B	3.46	3.53
C	3.95	4.02
D	2.97	
E	3.35	
F	2.17	
G	6.80	

[a] See Fig. 5.
[b] **2a$_{low}$** is defined as the conformer with the lowest CHARMm energy of the 50 calculated structures.
[c] Determined from X-ray crystallographic data. See Refs. [247,248].

(Fig. 5b), which resonates at 0.62 ppm (Fig. 2, inset). Insight regarding the origin of this large upfield shift for H_5 in compound **2a** is gleaned from metrical analysis of the calculated structure. The distance separating the H_5 nucleus from the porphyrin least squares plane in the calculated structure (F, Fig. 5b) is 2.17 Å. The upright orientation of the Naphthalene II pillar directs H_5 into the porphyrin core, where it is flanked on either side by the porphyryl 10 and 20 substituents.

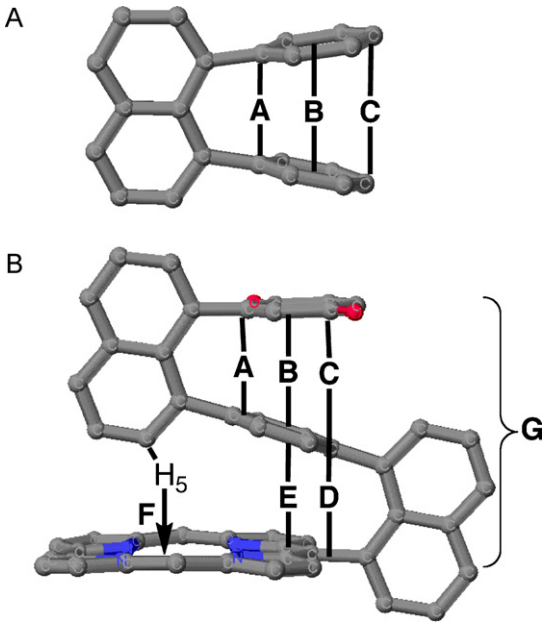

Fig. 5. Schematic highlighting the key interplanar distances in (a) 1,8-diphenylnaphthalene and (b) compound **2a** [246].

NMR data thus highlight that these uniquely rigid, π-stacked ET assemblies manifest interplanar distances between D, bridge, and A aromatic units in the condensed phase that are less than the sums of their respective van der Waals radii. The 1D ^{1}H NMR and 2D NMR data of these compounds show that: (i) the 1,8-naphthyl pillaring motif constrains nuclei to reside in unusual and diverse local magnetic environments, and (ii) the close contacts afforded by a sub van der Waals interplanar separation of D, Sp, and A give rise to a comprehensive set of structurally significant NOE signatures that can be used as constraints in quantitative structural calculations. Examination of such data using *ab initio* SA analysis shows that compound **2a** constitutes an unusual example for which these analytical tools unequivocally determine a single unique structure in solution.

3. Distance dependence of electron transfer rate constants

Studies that interrogate the distance dependence of the ET rate constant (the β value; Eq. (7)) are more common than studies that determine the distance dependent decay of the electronic coupling matrix element (the β^H value; Eq. (6)), as such analyses do not require the concomitant evaluation of the reaction free energy and the reorganization energy at each D–A distance; furthermore, such studies often define the initial experiments that are carried out to provide insight into the extent of electronic communication that exists within newly defined D–Sp–A structural motifs.

Congruent with this approach, we evaluated the photo-induced charge separation and the thermal charge recombination reaction rate constants for (**1**–**3**)**a-Zn** via pump-probe transient absorption spectroscopy. Protected-quinone derivatives of (**1**–**3**)**a-Zn** ([5-[8′-(2″,5″-dimethoxyphenyl)-1′-naphthyl]-10,20-diphenylporphinato]zinc(II) (**1M-Zn**), [5-[8′-(4″-[8‴-(2⁗,5⁗-dimethoxyphenyl)-1‴-naphthyl]-1″-phenyl)-1′-naphthyl]-10,20-diphenylporphinato]zinc(II) (**2M-Zn**), and [5-(8′-[4″-(8‴-[4⁗-(8⁗⁗-[2⁗⁗,5⁗⁗-dimethoxyphenyl]-1⁗⁗-naphthyl)-1⁗-phenyl]-1‴-naphthyl)-1″-phenyl]-1′-naphthyl)-10,20-diphenylporphinato]zinc(II) (**3M-Zn**)) served as key spectroscopic benchmarks for this study (Fig. 6) [149]. For example, a transient spectrum obtained at 193 fs time delay for **2a-Zn** in CH_2Cl_2 following Q-band excitation reflects the difference spectrum of the singlet-excited state, resembling the S_1 state spectrum obtained for **2M-Zn** and simple (porphinato)zinc (II) (PZn) species (data not shown). This spectrum evolves with time; the spectral signature of an intermediate state is clearly evident at a delay time of 1 ps. No further spectral evolution is evident at delay times >1 ps; transient signals at all wavelengths

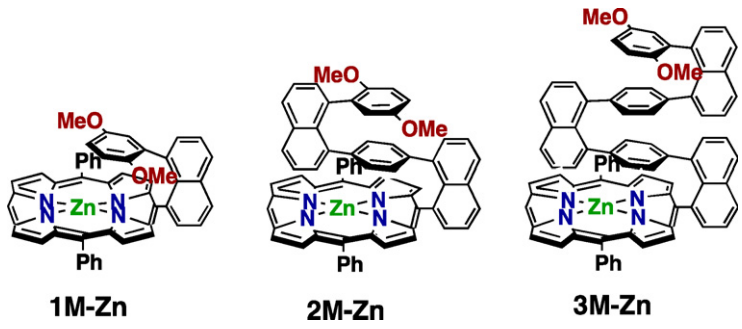

Fig. 6. Structure of protected ([5-[8′-(2″,5″-dimethoxyphenyl)-1′-naphthyl]-10,20-diphenylporphinato]zinc(II) (**1M-Zn**), [5-[8′-(4″-[8‴-(2⁗,5⁗-dimethoxyphenyl)-1‴-naphthyl]-1″-phenyl)-1′-naphthyl]-10,20-diphenylporphinato]zinc(II) (**2M-Zn**), and [5-(8′-[4″-(8‴-[4⁗-(8⁗⁗-[2⁗⁗,5⁗⁗-dimethoxyphenyl]-1⁗⁗-naphthyl)-1⁗-phenyl]-1‴-naphthyl)-1″-phenyl]-1′-naphthyl)-10,20-diphenylporphinato]zinc(II) (**3M-Zn**).

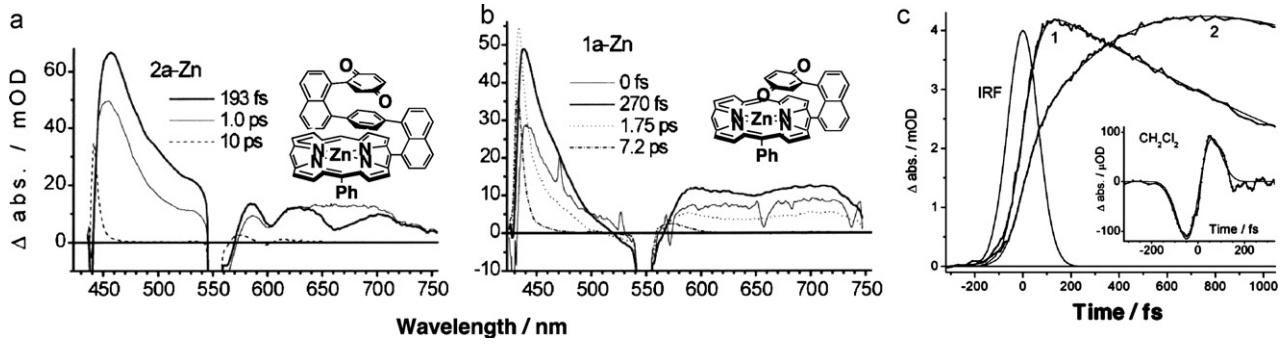

Fig. 7. Transient absorption spectra of **2a-Zn** (a) and **1a-Zn** (b). Time delays are shown as insets. (c) Kinetics for **1a-Zn** (1) and **2a-Zn** (2) measured at 650 nm, along with the instrument response function (IRF); λ_{ex} = 557 nm, temperature = 23 ± 1 °C. The response of the pure solvent (CH_2Cl_2) measured at the same wavelength is shown in the inset.

decay concomitantly (Fig. 7). The spectrum of the intermediate has a pronounced band around 650–700 nm, characteristic of the (porphinato)zinc (II) cation radical ($PZn^{\bullet+}$) [249]. Similar time-dependent spectra were observed for **3a-Zn**. The respective CS time constants for **2a-Zn** and **3a-Zn** were determined to be 0.62 ± 0.02 and 3.1 ± 0.3 ps (Fig. 7).

The nature of the ET dynamics following excitation in **1a-Zn** differs with respect to that delineated for (**2**–**3**)**a-Zn** (Fig. 7). The initial spectrum (t = 270 fs) decays essentially without change over the wide spectral window (λ: 480–530 nm, >610 nm). Since the transient spectrum appears similar to that for (5,10,15,20-tetraphenylporphinato)zinc(II) (**TPPZn**) cation radical, showing the characteristic absorption band at long wavelengths (~680 nm) [249], the observed transient spectrum evident in Fig. 7 for **1a-Zn** was assigned to the charge separated $PZn^{\bullet+}Q^{\bullet-}$ state. Thus, the observed decay of the absorption envelope centered at 680 nm corresponds to the CR reaction. The CS reaction could not be resolved within the time resolution of our experimental apparatus with multichannel detection. Note that the zero-time spectrum shown in Fig. 7 is similar to the spectrum obtained at a time delay of a 270 fs; an exact comparison of these spectra, however, is complicated by a nonlinear solvent contribution and Raman scattering peaks around zero time. To estimate the CS rate constant for **1a-Zn**, we carried out pump-probe experiments using single wavelength detection: fitting the signal observed at 650 nm (Fig. 7C) as a biexponential convoluted with the instrument response function (IRF, 150 ± 5 fs), enables an estimate of $\tau_{CS} \leq 20$ fs. Note that the observed charge-separated states for **1a-Zn**, **2a-Zn**, and **3a-Zn** undergo rapid charge recombination reactions τ_{CR} = 1.6 ± 0.2, 1.7 ± 0.1, and 20 ± 2 ps, respectively.

Fig. 8 highlights the distance dependence of the CS and CR rate constants for the **1a-Zn**, **2a-Zn**, and **3a-Zn** ET systems. The CS rate constant determined for **1a-Zn** was not factored into our computation of β_{CS} because the magnitude of the ET rate constant for CS in **1a-Zn** greatly exceeds that of the fastest component of solvent relaxation (~10^{13} s^{-1}) [250], and thus it was considered adiabatic. Taking the extensive data sets of distance and driving force-dependent ET rate data compiled by Lewis and Wasielewski as benchmarks [180–182,251], it is clear that the magnitude of the phenomenological ET distance dependence (β) for both the CS and CR reactions in these systems (β_{CS} = 0.43 $Å^{-1}$; β_{CR} = 0.35 ± 0.16 $Å^{-1}$) is approximately a factor of two smaller than that determined in

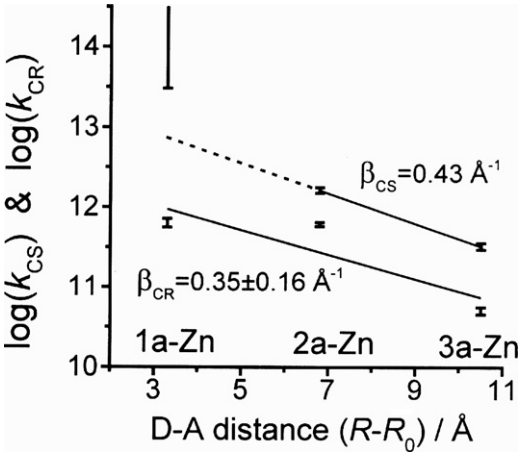

Fig. 8. Distance dependence of the CS and CR rate constants for (**1**–**3**)**a-Zn** in methylene chloride at 23 ± 1 °C. Slopes of the straight line plots shown give β_{CR} = 0.35 ± 0.16 $Å^{-1}$ (CR) and β_{CS} = 0.43 $Å^{-1}$ (CS) [R_0 = 2.97 Å; k_0 = 1.1 × 10^{12} s^{-1} (CR); k_0 = 8.5 × 10^{13} s^{-1} (CS)]. Given the adiabatic nature of CS in **1a-Zn**, β_{CS} was computed using the relevant data points for **2a-Zn** and **3a-Zn** only. Error bars for each experimental rate constant are shown. Note that the lower limit of the error bar for the CS rate constant of **1a-Zn** corresponds to the fastest rate constant that we can resolve (5 × 10^{13} s^{-1}); the width of this error bar is arbitrary. The error reported in β_{CR} was determined via standard linear regression analysis [149].

D/A-modified DNA hairpin structures (β_{CS} = 0.7 Å^{-1}; β_{CR} = 0.9 Å^{-1}) [182]; interestingly, the magnitude of these decay parameters is reminiscent of those determined for several classes of highly conjugated organic structures [70,157,158,164,252].

For DNA-based D–Sp–A systems in which a wide range of β values were observed (0.1–1.5 Å^{-1}), Lewis and coworkers provided a interesting linear relationship between the electron injection free energy (ΔG_{inj}) and the decay parameter (β). ΔG_{inj} is defined as the minimum free energy difference between the state with the hole localized on the bridge (A^-B^+D) and the initial (A^*BD) or final state (A^-BD^+), which is closely related to the tunneling energy gap, yet easily estimated by electrochemical measurements. In these systems, A^*BD is the reactant state, with the virtual intermediate thus A^-B^+D; the tunneling energy gap can be defined as $\Delta E_{tun} = E_{tun} - (-IP)$. The role of the tunneling energy gap is well explained within the context of the McConnell model [68]. Briefly, the McConnell model assumes that the bridge consists of a periodic chain of orbitals with nearest neighbor interaction elements, t_{min}, and energy gap, ΔE, between the donor and bridge localized orbitals, such that

$$\beta^H = \frac{2}{R_0} \ln \left| \frac{\Delta E_{tun} + 2|t_{min}|}{t_{min}} \right|$$

Since the tunneling energies are derived from the properties of the (nonequilibrium) activated complex and thus are difficult to determine experimentally, the value for ΔG_{inj} is utilized computationally instead of ΔE_{tun} [68]. According to this analysis, a 0.25–0.50 eV change in ΔG_{inj} gives rise to a 0.7–1.1 Å^{-1} of the decay parameter. Given an approximate ΔG_{inj} value for **2a-Zn** of 2.35 eV, the experimental distance dependence for CS (β = 0.43 Å^{-1}) is nearly a factor of two smaller than that predicted by this model (β = 0.7–1.1 Å^{-1}), suggesting that sub van der Waals interplanar separations that exist between D, Sp, and A units in **1**–**3a-Zn** play a prominent role in augmenting the magnitude of D–A electronic coupling relative to that provided by DNA for similar ΔG_{inj} values.

4. Electron transfer mechanism

In the above section, we overviewed the distance dependence of the CS and CR rate constants in these rigid, cofacially compressed, π-stacked porphyrin–bridge–quinone systems. Calculation of the electronic coupling matrix element from ET rate constant data often utilizes the quantum mechanical nonadiabatic ET rate equation (Eq. (3)). This analysis implies that any ET process analyzed should indeed be nonadiabatic in nature, with an electronic coupling matrix element small enough in magnitude to guarantee that the reaction lies in the perturbation limit. For example, exclusion of the **1a-Zn** CS rate constant, in which the estimated electronic coupling is ~1000 cm^{-1}, is appropriate for data analysis based on Eq. (3). In addition, any ET reaction analyzed using the quantum mechanical nonadiabatic ET expression should also be insensitive to the solvent dynamics. If not, a more rigorous theoretical framework is necessary for the analysis of electronic coupling; hence, appropriate insight into the ET reaction to be analyzed is a prerequisite for obtaining a physically meaningful value of the electronic coupling matrix element.

Likewise, computation of H_{DA}^2 from ET rate constant data is sensitive to reorganization energy and reaction free energy values; as these parameters enter into the exponential term, the manner in which they are evaluated is critical. The following section describes how these parameters were determined at various D–A distances and temperatures for **1**–**3a-Zn** and closely related structures.

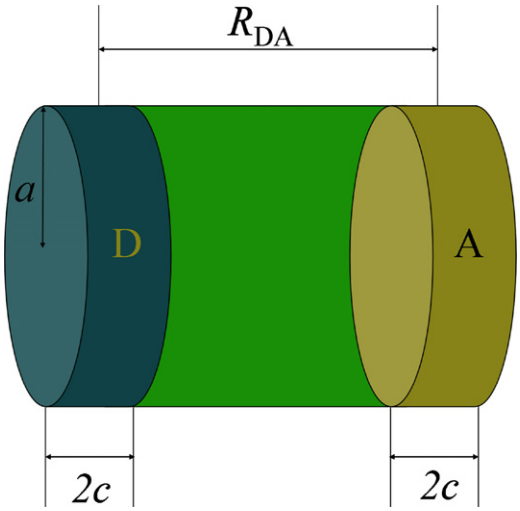

Fig. 9. Solvent reorganization energies calculated by the modified dielectric continuum model described by Kato and Tachiya [253]. The overall molecular shape is assumed to be a cylinder having a 4.9 Å diameter and 10.61 Å length (2c R_{DA}, where c is the half of the van der Waals thickness (1.75 Å) of porphyrin or quinone and R_{DA} is the porphyrin plane-to-quinonyl centroid distances (7.11 Å) for DFT optimized structures) [127].

4.1. Estimation of reorganization and reaction free energies

4.1.1. Inner and outer sphere reorganization energies

The outer sphere reorganization energy λ_o, is estimated commonly via the classic Marcus expression, where a spherical donor and acceptor are assumed to be imbedded in a dielectric continuum [54];

$$\lambda_S = \frac{e^2}{4\pi\varepsilon_0} \left(\frac{1}{\varepsilon_{op}} - \frac{1}{\varepsilon_S} \right) \left(\frac{1}{2R_D} + \frac{1}{2R_A} - \frac{1}{R_{DA}} \right) \quad (8)$$

where ε_{op} and ε_s are respective optical and static dielectric constants of the solvent, R_{DA} is the D–A distance, and R_D and R_A are the respective donor and acceptor ionic radii. For an ET system where the D and A separation distance is much larger than the sum of the D and A van der Waals radii, Eq. (8) can be used without restriction. In (**1**–**3**)**a-Zn** there are no solvent molecules directly intervening between D and A, due to the sub-van der Waals contact distances that exist between D–A (**1a-Zn**), and between D–bridge and bridge–A [(**2**–**3a**)**-Zn**]. Kato and Tachiya considered such a case; they treated D and A as disks, with or without an intervening spacer structure, and aligned D, A, and bridge units in a stacked manner. Eq. (9) summarizes the Kato and Tachiya analysis [253], while Fig. 9 provides a graphical representation of the parameters that have not yet been defined.

$$\lambda_s = \frac{e^2}{4} \left(\frac{1}{\varepsilon_{op}} - \frac{1}{\varepsilon_s} \right) \left[\left(\frac{1}{c} + \frac{2}{R_{DA}+c} - \frac{4}{R_{DA}+2c} \right) + \frac{1}{a} \left(\tan^{-1} \frac{R_{DA}+c}{a} + \tan^{-1} \frac{c}{a} \right) - \int_{-((R_{DA})/2)-c}^{((R_{DA})/2)+c} \frac{2a^2}{f(x)(f(x)+a^2-x^2+(R_{DA}^2/4))} dx \right]$$
$$f(x) = \sqrt{a^4 + 2\left(x^2 + \frac{R_{DA}^2}{4}\right)a^2 + \left(x^2 - \frac{R_{DA}^2}{4}\right)^2} \quad (9)$$

It is important to note that reorganization energies calculated within the context of this model are 20–30% smaller than that arrived at through the Marcus expression. The Kato and Tachiya analysis gives a reasonable magnitude outer sphere reorganization energy for **1a-Zn**; in contrast, note that Eq. (8) would predict a phys-

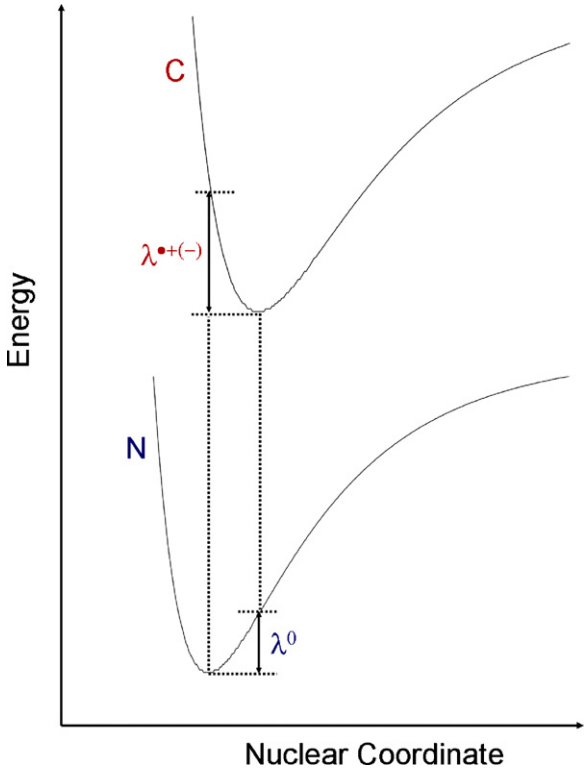

Fig. 10. Potential energy surface for neutral (N) and charged (C) states that define λ^0 and $\lambda^{\bullet+}_{i,p}$ ($\lambda^{\bullet-}_{i,p}$).

ically unreasonable, negative outer sphere reorganization energy for this D–A assembly. Kato–Tachiya outer sphere reorganization energies were used in the analysis of the ET rate data obtained for the (**1**–**3**)**a-Zn** systems.

The inner-sphere reorganization energy λ_i can be expressed as the sum of the reorganization energy of the initial neutral D (A), λ^0, and the reorganization energy of the corresponding radical cation (anion), $\lambda^{\bullet+}_{i,p}$ ($\lambda^{\bullet-}_{i,p}$). This relation is illustrated in Fig. 10 [254]. From this expression, the total inner-sphere reorganization energy for (**1**–**3**)**a-Zn** systems was estimated using the following equations:

$$\lambda_i = \lambda_{i,p} + \lambda_{i,q} \tag{10}$$

$$\lambda_{i,p} = \lambda^0_{i,p} + \lambda^{\bullet+}_{i,p},\ \lambda_{i,q} = \lambda^0_{i,q} + \lambda^{\bullet-}_{i,p} \tag{11}$$

where superscripts p and q denote porphyrin and benzoquinone, respectively. A recent report by Amashukeli provides the inner-sphere reorganization energies of several (porphinato)zinc(II) complexes determined from the first ionization potentials obtained via gas-phase valence photoelectron spectroscopy [254]. Importantly, experimentally determined λ_i values indicate that structural changes that occur concomitant with oxidation are largely confined to the porphyrin ring, with macrocycle peripheral substituents, solvent, and other environmental factors making significantly smaller contributions to the total inner-sphere reorganization energy. The experimentally determined (porphinato)zinc(II) λ_i values were found to range between 0.12 and 0.14 eV, which compared well to computationally derived values from methods utilizing a mixture of Hartree–Fock exchange and DFT exchange-correlation functionals [254].

The inner-sphere reorganization energy of benzoquinone was found to be 0.35 eV, determined from a DFT calculation utilizing the BH and HLYP hybrid functional and 6-31g(d) basis set implemented in the Gaussian03 program package [255]. Combined with the inner-sphere reorganization energy of the (porphinato)zinc(II) unit from the literature [254], the total inner-sphere reorganization energies of (**1**–**3**)**a-Zn** systems are estimated to be ~0.5 eV.

4.1.2. Temperature dependence of the reorganization energy and the reaction free energy

Liang, Miller, and Closs reported the temperature dependence of long-range ET reactions in the Marcus inverted region, where ET rates were independent, or negatively dependent, on temperature [256,257]. These results were interpreted as having their genesis from a nuclear tunneling effect, after appropriate account of the temperature dependence of reorganization energy and driving force was made.

The temperature dependence of reorganization energy derives mainly from the temperature dependence of the outer-sphere reorganization energy, which originates with the temperature sensitivity of the high frequency dielectric (ε_{op}) and static dielectric (ε_s) constants.

ε_{op} can be expressed as a function of temperature [258]; from the Lorentz–Lorentz expression, the molar refractivity, ρ, is described as

$$\rho(T) = \left(\frac{\varepsilon_{op}(T) - 1}{\varepsilon_{op}(T) + 2}\right)\frac{M}{d_{20}} \tag{12}$$

where M is the molecular weight and d is the density at the 20 °C [259].

$$\varepsilon_{op}(T) = \left(\frac{M + 2d_{20}\rho(T)}{M - d_{20}\rho(T)}\right) \tag{13}$$

The temperature dependent density of the solvent can thus be obtained from literature values. For example [260],

$$\rho(T) = 1157 - 1.124T + 2.54 \times 10^{-4}T^2 \quad \text{for 2-methyl-3, 3, 4, 4 -tetrahydrofuran (2_MTHF)} \tag{14}$$

$$\rho(T) = -0.001T + 0.8859 \quad \text{for toluene} \tag{15}$$

Note that the static dielectric constants of many solvents as a function of temperature have been experimentally determined [258]. For 2-MTHF,

$$\varepsilon_s(T) = 3.1 + \frac{860}{T - 73}\ (> 140\,\text{K}),\ \varepsilon_s(T) = 2.6 \pm 0.1\ (< 90\,\text{K}) \tag{16}$$

while for toluene, a relation obtained through linear regression analysis of experimental data was used.

$$\varepsilon_s(T) = -0.0035T + 2.4446 \tag{17}$$

The thermodynamic driving forces for charge separation and charge recombination reactions were calculated using Eqs. (18) and (19).

$$\Delta G_{CS} = e(E_{ox} - E_{red}) - E_{00} - \frac{e^2}{4\pi\varepsilon_0\varepsilon_S R_{DA}} + \frac{e^2}{4\pi\varepsilon_0}\left(\frac{1}{\varepsilon_S} - \frac{1}{\varepsilon_S^{ref}}\right) \times \left(\frac{1}{2R_D} + \frac{1}{2R_A}\right) \tag{18}$$

$$\Delta G_{CR} = -\Delta G_{CS} - E_{00} \tag{19}$$

where E_{ox} and E_{red} are the respective donor and acceptor redox potentials, E_{00} is the zero energy of the excited molecule, ε_S is the solvent dielectric constant, ε_S^{ref} is the dielectric constant of the solvent in which redox potentials were measured, and R_{DA}, R_D, and R_A are defined as described in Eq. (8). E_{00} energies were determined from electronic absorption and fluorescence emission spectral experiments. Note that the magnitude of the static dielectric constant plays a major role in determining the temperature dependence of the reaction free energy.

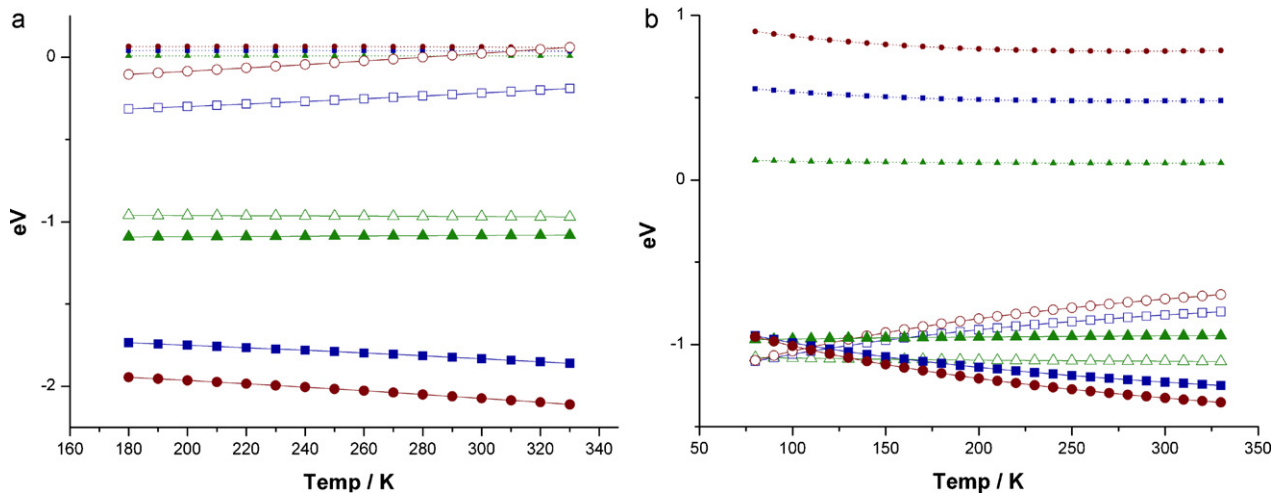

Fig. 11. Temperature dependence of the outer-sphere reorganization (small circles, squares, triangles; dotted lines) and reaction free energies (larger circles, squares, triangles; solid lines) of **1a-Zn** (green), **2a-Zn** (dark blue), and **3a-Zn** (dark red) in toluene (a) and 2-MTHF (b). Open and closed symbols represent CS and CR reactions, respectively.

Fig. 11 describes the temperature dependence of the outer-sphere reorganization energy and the reaction free energy of (**1**–**3**)**a-Zn** in toluene (Fig. 11a) and 2-MTHF (Fig. 11b). In these systems, the magnitude of the outer-sphere reorganization energy is almost temperature independent over a 80–330 K range in 2-MTHF solvent; a similar temperature dependence is observed over 180–330 K in toluene. In contrast, the reaction free energy shows a clear temperature dependence, which is more pronounced in 2-MTHF. This temperature dependence of the reaction free energy increases with the size of the D–Sp–A assembly, and gives rise to an unusual temperature dependence of the magnitude of the ET rate constant; one such example is illustrated in Fig. 12. Note that as the temperature decreases, the CS reaction free energy of **3a-Zn** shifts to a more negative value. If the ET mechanism remains in the nonadiabatic super-exchange limit over the experimental temperature window, the Marcus expression (Eq. (1)) predicts a mild decrease of the ET rate constant with decreasing temperature. In contrast, a simple QM treatment (Eq. (3)) of the data predicts a slight increase in the magnitude of k_{ET} with decreasing T, which is often referred to as a negative temperature dependence. If the reaction free energy remains constant over the experimental temperature domain, both the Marcus and QM ET rate expressions predict sharp decreases of k_{ET} with temperature. Similar dependences of k_{ET} upon T are manifest for the CR reaction for each of these theoretical treatments (Fig. 12b), due to the temperature dependence of the reaction free energy. A comparison between the experimentally determined dependence of the magnitude of k_{CS} with temperature, with that predicted theoretically by the QM model, is shown in Fig. 13.

4.2. *The temperature dependence of **2a-Zn** electron transfer dynamics in 2-methyl-3,3,4,4-tetrahydrofuran (2-MTHF)*

Eq. (1) can be interpreted as a classical transition state rate equation. As the activation energy and the preexponential factor can be extracted from the Arrhenius equation, Eq. (1) can be recast in the form [256,261–263]

$$\ln(k_{ET}\sqrt{T}) = \ln\left(\frac{2\pi}{\hbar}\frac{H_{DA}^2}{\sqrt{4\pi\lambda_T k_B}}\right) - \frac{(\Delta G + \lambda_T)^2}{4\lambda_T k_B}\frac{1}{T} \quad (20)$$

From this analysis, H_{DA} can be extracted with following determination of λ_T.

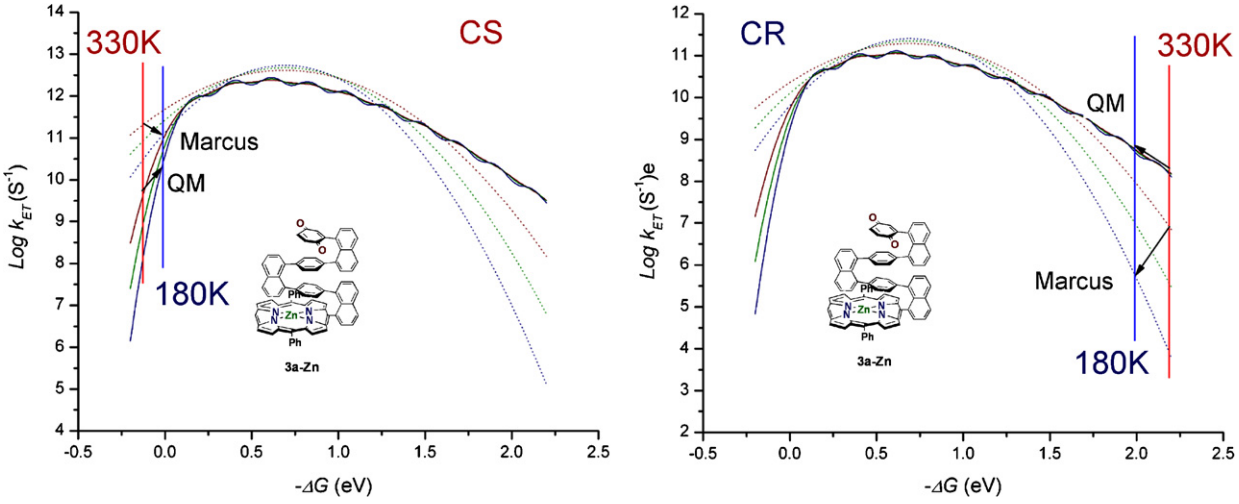

Fig. 12. The impact of the temperature dependence of the reaction free energy upon the magnitude of the ET rate constant for **3a-Zn** in toluene solvent. The dotted and solid lines represent the log(k_{ET}) vs. ΔG relation predicted by Marcus (Eq. (1)) and QM (Eq. (3)) rate equations, respectively, at 330 K (red), 250 K (green), and 180 K (blue). Vertical lines are displayed as visual guides.

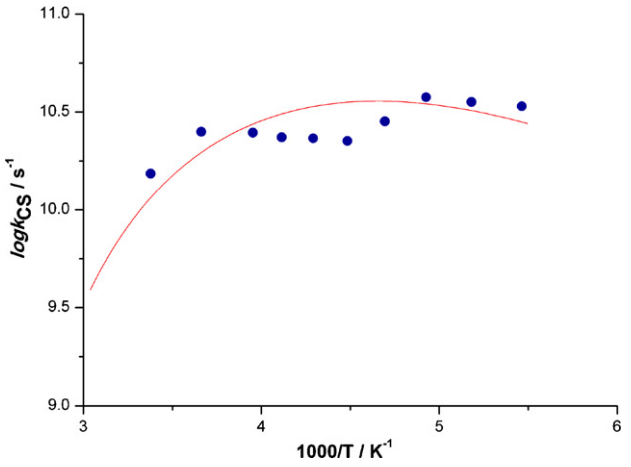

Fig. 13. Comparison of the experimentally determined k_{CS} values (filled blue circles) for **3a-Zn** with that predicted theoretically using the QM model (Eq. (3); red line). Note that this analysis takes into account the temperature dependence of the inner- and outer-sphere reorganization and reaction free energies.

Based on the strategy described above, we measured photoinduced CS rate constants for **2a-Zn** in 2-MTHF solvent over an 80–320 K temperature range. Spectral evolution following photoexcitation at 557 nm at three representative temperatures (310, 120, and 80 K) were very similar to those observed in CH_2Cl_2 solvent. Fig. 14 highlights the comparative decay kinetics of the transient absorption spectra probed at 658 nm. At temperatures higher than 150 K, these transient decay kinetics were fit nicely by biexponential functions with similar amplitudes for the rise and the decay components (Eq. (21)). Below 150 K, however, fitting with a biexponential function yielded results that became increasingly poor with decreasing temperature. In this low temperature region, only by using a triexponential function with two rising components and one decaying component could the data be satisfactorily modeled (Eq. (22)). The slower rising component (k_1, τ_1) exhibited an unusual temperature dependence while the faster one (k_2, τ_2) was nearly temperature independent over all temperature ranges. It is important to note that the ratio of amplitudes of these two components (A_1/A_2, $\tau_1 > \tau_2$) became smaller as the temperature decreased [152]. The sole decay component (τ_3) is assigned as CR in these cases.

$$CS(t) = A_0 + A_1 \exp\left(\frac{-\tau_1}{t}\right) + A_3 \exp\left(\frac{-\tau_3}{t}\right) \quad (21)$$

$$CS(t) = A_0 + A_1 \exp\left(\frac{-\tau_1}{t}\right) + A_2 \exp\left(\frac{-\tau_2}{t}\right) + A_3 \exp(-\tau_3 t) \quad (22)$$

Our initial interpretation for the temperature-independent k_2 component corresponded to that for a nuclear tunneling or a barrierless crossing, both of which do not necessarily overcome the activation barrier and thus do not give rise to a temperature dependence. Note that the k_1 component, however, exhibited a weak temperature dependence at relatively high temperature ($T \geq 270$ K), but was subject to a severe temperature dependence over the 260–150 K range, while departing this pattern in the low temperature region ($T < 150$ K). To elucidate the nature of the temperature dependence of the k_1 rising component evident in the excited-state transient dynamics of **2a-Zn**, we analyzed these data within the context of several established ET theories, which are discussed in the following sections.

4.3. The impact of high frequency vibrational acceptor modes upon electron transfer dynamics

In addition to the classical ET rate equation (Eq. (1)), we also considered the quantum mechanical rate expression (Eq. (3)). The main difference between Eqs. (1) and (3) is a Franck-Condon (FC) factor; note that the sum of products of overlap integrals of the equilibrated vibrational wave functions of the reactant state with multiple, averaged high frequency vibrational wavefunctions of the product state, is taken into account in Eq. (3). In the Marcus normal region, both classical and quantum mechanical models predict an Arrhenius-type temperature dependence of k_{ET} in the high temperature limit ($k_BT \gg \langle\hbar\omega\rangle$). In the low temperature limit ($k_BT \ll \langle\hbar\omega\rangle$), however, the Poisson-type function ($k_{ET} \propto \exp(-S_c)S_c^n/n!$) prevails and the temperature dependence of ET reaction rate constants become very weak. It is important to note that both classical and quantum mechanical models predict a weak temperature dependence of the ET rate constant for the case where the energetics restrict the system to the Marcus activationless or inverted region, even in the high temperature limit. The temperature dependence of the **2a-Zn** CS reaction in 2-MTHF is such a case; the relationship between the experimental temperature dependence of k_{CS} and that predicted via these theoretical models is illustrated in Fig. 15.

The temperature independent k_2 component is described well by analyses utilizing both classical Marcus and QM theoretical treatments. Note, however, that the k_1 component is not readily rationalized within the context of either of these models.

4.4. Coupling charge transfer and solvation dynamics; the solvent controlled adiabatic reaction

When the ET dynamics are coupled to the solvent dynamics, the temperature-dependent description of the ET rate constant requires a more sophisticated approach. Dynamical solvent effects are usually discussed from a collisional or dielectric point of view [264]; the latter has attracted much attention in connection with the ET reaction. The extent to which solvent dynamics influence ET reactions depends on the nature of the solute-solvent interaction, which is electrostatic in origin. Since an intramolecular ET reaction is accompanied by a drastic change in molecular polarity, an ET reaction is more likely to be coupled to the motion of polar solvent molecules [265–269]. A theoretical treatment of this type of ET reaction is based on the Zusman's stochastic Liouville equation approach; following experimental verification, this mechanism has been termed as the solvent-controlled adiabatic reaction

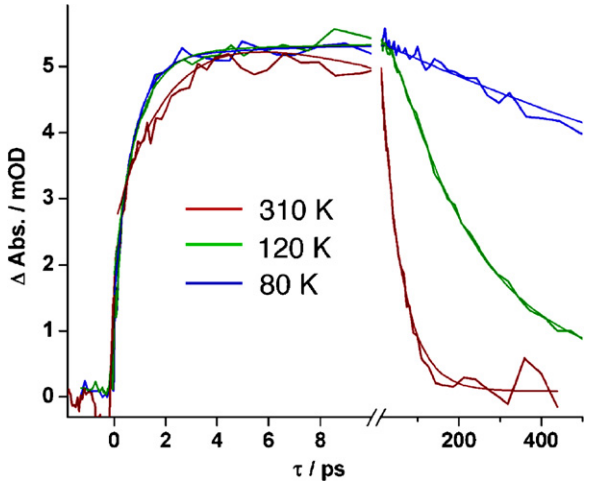

Fig. 14. Normalized transient decay kinetics determined at 658 nm following optical excitation of **2a-Zn**. The best biexponential function fit for 310 K and the triexponential function fits for 120 K and 80 K are depicted by thin lines. Experimental conditions: λ_{ex} = 557 nm, solvent = 2-MTHF, magic angle polarization [152].

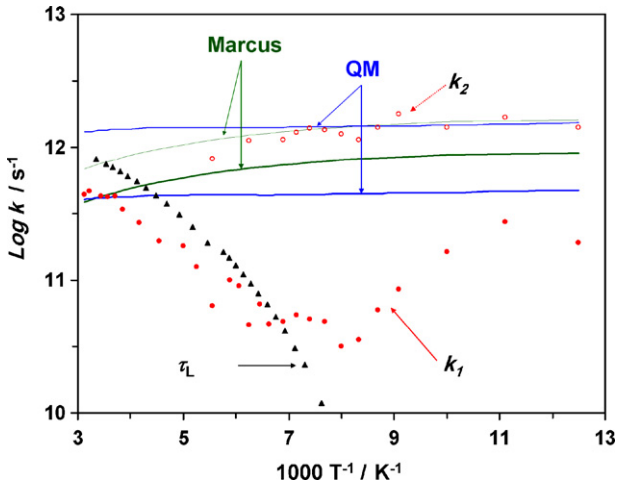

Fig. 15. Comparison of the experimental temperature dependence of the two CS rate constants (filled red circles = k_1; open red circles = k_2) evident in the transient dynamics observed for electronically excited **2a-Zn**, with those calculated via Marcus (green thin and thick lines for H_{DA} = 60 and 45 cm^{-1}, respectively) and QM (blue thin and thick lines for H_{DA} = 90 and 50 cm^{-1}, respectively) models. The temperature dependence of the outer-sphere reorganization energy (λ_o) and reaction free energy (ΔG) were taken into account in these theoretical analyses [256,259]. For the QM calculation, an inner-sphere reorganization energy λ_i = 0.5 eV and an averaged single high-frequency vibrational quantum $\hbar\langle\omega\rangle$ = 1600 cm^{-1} were used. The temperature dependent inverse longitudinal relaxation times of 2-MTHF (τ_L^{-1}) are shown as black triangles [152].

[204,270–282]. One important issue regarding this ET mechanism is the timescale relation between the solvent dynamics and the ET event. When the ET reaction timescale is much slower than that of solvent dynamics, the ET rate constant is governed mainly by the electronic tunneling probability at a given driving force, and is thus nonadiabatic. When the ET rate constant is comparable to or faster than that for solvent dynamics, the solvent controlled adiabatic mechanism prevails; only in this case does the timescale at which the reactant system approaches the transition state become rate-determined by solvent friction. The transition from a nonadiabatic to a solvent controlled adiabatic ET reaction mechanism is thus possible when the timescale of the ET reaction has relatively weak temperature dependence, and coincides with that of solvent dynamics [283–287].

An Arrhenius type temperature dependence appeared to be displayed in the medium-to-high temperature region (T > 150 K), where the **2a-Zn** CS reaction is well described by a mono-exponential decay profile. A $\ln(k\sqrt{T})$ vs. T^{-1} plot of the data in this

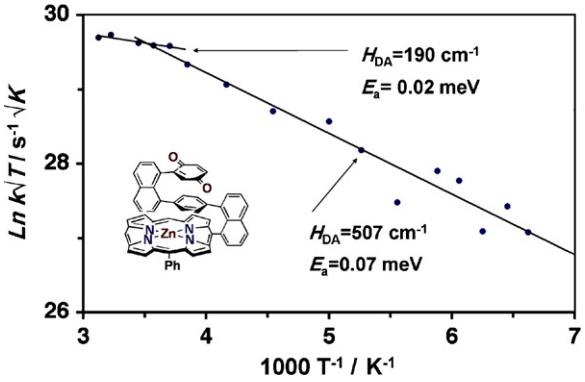

Fig. 16. Arrhenius analysis of the k_1 CS rate constant observed in the excited-state **2a-Zn** transient dynamics. Deduced electronic coupling matrix elements and activation barriers for the two apparent linear regimes are shown as insets [152].

temperature region suggests two different linear regimes (Fig. 16); the activation barriers for these two regions were evaluated to be 0.51 and 1.62 kcal/mol for the high (260 K < T < 320 K) and medium (150 K < T < 260 K) temperature domains, respectively. Electronic coupling matrix elements (H_{DA}) were determined in this analysis to be 190 and 503 cm^{-1} for the high and medium temperature regions. Whether these values represent the actual electronic coupling is an open question, as the analysis employing Eq. (20) is based on the assumption that the total reorganization energy and the reaction free energy are constant within the relevant temperature region. The outer-sphere reorganization energies for **2a-Zn** were found to be relatively invariant over the 150–320 K temperature domain (0.48 < λ_T < 0.50); in contrast, the reaction free energies were temperature dependent, ranging from −0.81 eV at 320 K to −0.97 eV at 150 K. Furthermore, these simple analyses suggest a >2-fold increase in the evaluated magnitudes of H_{DA} with an ~100 K decrease in temperature. Considering the fact that both Marcus and QM theories predict very similar electronic coupling values for the CS reactions (45–50 cm^{-1}), the extracted 503 cm^{-1} value for H_{DA} in the medium temperature region for **2a-Zn** suggests that the apparent temperature dependence cannot be attributed exclusively to a thermal activation barrier.

Interestingly, the temperature-dependent component of the experimental ET dynamics (k_1) in the medium temperature region was found to mimic the sharply decreasing pattern of the solvent longitudinal relaxation rate constants (τ_L^{-1}) (Fig. 15), suggesting that in this temperature region the CS reaction is strongly coupled to the solvent dynamics. To further probe this possibility, we simulated experimental ET rate constants using the theoretical framework developed by Rips and Jortner [276–278]. The ET rate constant in the solvent controlled adiabatic regime can be expressed as

$$k_{SC} = \frac{k_{NA}}{(1+\kappa_A)^{\gamma}} \tag{23}$$

$$\kappa_A = \frac{4\pi H_{DA}^2 \tau_L}{\hbar\lambda_o} \tag{24}$$

where k_{NA} is the nonadiabatic ET rate from the Eq. (3), κ_A is the adiabaticity parameter, and γ is the solvent dielectric relaxation parameter from the Davidson–Cole dielectric relaxation spectrum (Eq. (25)) [288,289].

$$\hat{\varepsilon}(\omega) = \varepsilon_\infty + \frac{\varepsilon_0 - \varepsilon_\infty}{(1+i\omega\tau_0)^{\gamma}} \tag{25}$$

The simulated k_{SC} values utilizing a γ value of 1 are plotted along with experimental k_1 data in Fig. 17. This model features a moderate-to-large solvent adiabaticity parameter ($2.0_{T=260} < \kappa_A < 19.6_{T=150}$, Eq. (24)); although the predicted k_{SC} values overestimate the solvent controlled adiabatic effect [290], and thus γ should be a value less than 1, this analysis showed a close relationship between the experimental results and that predicted using the solvent controlled adiabatic theoretical treatment described by Rips and Jortner [276–278].

It is appropriate to mention that solvent-controlled adiabatic ET reactions are expected to occur more commonly in the normal region, as in the activationless and inverted regimes ET events can be promoted by quantum-mechanical nuclear tunneling, which are little influenced by solvent dynamics [66,67]. In **2a-Zn**, the magnitude of the computed reaction free energy (ΔG = −0.81 eV) at 320 K is indeed ~0.17 eV smaller than the total reorganization energy (λ_s = 0.48 eV, λ_v = 0.5 eV), suggesting that the CS reaction resides within the Marcus normal region. ΔG_{CS} changes smoothly with decreasing temperature, and drives the reaction from the activationless region (T ~ 120–125 K) to the inverted region at temperatures below 120 K. For this reason, the magnitude of k_1 is

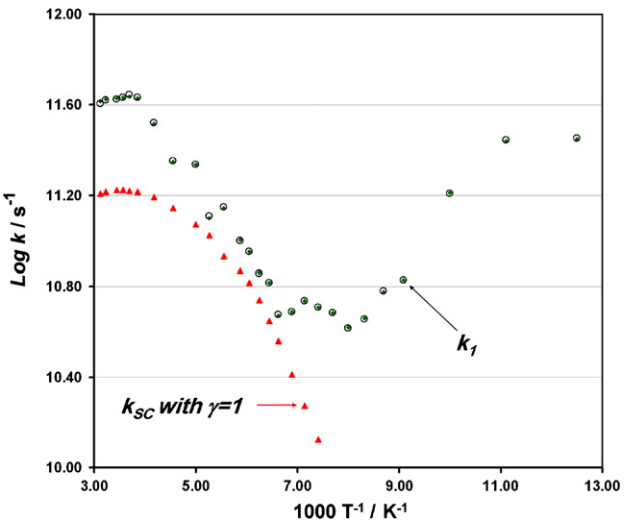

Fig. 17. Comparison of experimental temperature dependence of the CS rate constant (green diamonds with circle) with those calculated with the Rips/Jortner Model (Eq. (23)). For the calculation of k_{NA}, Eq. (3) was used, and H_{DA} was fixed at 46 cm^{-1}. Red triangles represent simulated charge-separation rate constants computed with a solvent dielectric relaxation parameter $\gamma = 1$.

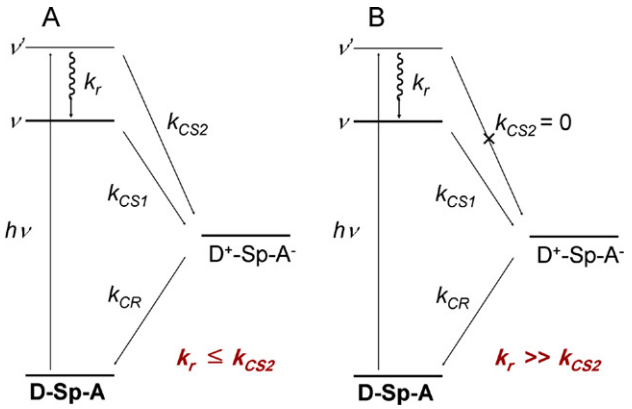

Fig. 18. Reaction schemes describing: (a) vibrational relaxation and electron transfer from a vibrationally excited S_1 state, and (b) an identical CS reaction but with no contribution from CS_2.

minimally affected by the solvent degrees of freedom at temperatures below 120 K, and a departure from the solvent controlled adiabatic regime for the CS reaction is manifest [291].

4.5. Electron transfer reactions involving vibrationally unequilibrated reactant states

As noted earlier, below 150 K the amplitude of the k_2 CS component increased relative to the temperature-dependent k_1 CS component. Deduced H_{DA} values for the temperature-independent k_2 CS reaction using Marcus and QM models were 60 and 64 cm^{-1}, respectively. These electronic coupling matrix elements computed with the same models used to evaluate the k_1 component were determined to be 46 and 36 cm^{-1}. With respect to the larger magnitude H_{DA} value determined for k_2, note that the timescale of the k_2 component is comparable to that for vibrational relaxation in the (porphinato)zinc(II) S_1 state manifold [292–297].

As the **^{1}2a-Zn*** state was prepared using laser excitation having excess energy (~0.17 eV) relative to the $S_0(\nu = 0) \rightarrow S_1(\nu = 0)$ transition, a competition between vibronic relaxation to an equilibrated S_1 state and direct ET to the CS state from the vibrationally unrelaxed **^{1}2a-Zn*** state without influence of the solvent coordinate, is possible. While there have been a number of reports that emphasized the competition between vibrational relaxation and electron transfer within the excited state manifold [298], relatively few studies have probed such competitive dynamics for ultrafast charge separation or injection [299–304]. Fig. 18a describes a scenario where ET from the vibrationally unrelaxed **2a-Zn** singlet excited state occurs faster or comparable to the S_1 vibrational manifold relaxation rate. Based on the reaction scheme in Fig. 18a, the kinetics of transient decay of CS state are given by Eq. (26):

$$CS(t) = A_0[A_1 \exp(-k_e t) + A_2 \exp(-k_{CS1} t) + A_3 \exp(-k_{CR} t)] + C \quad (26)$$

Here, $k_e = k_r + k_{CS2}$, $A_1 = [k_{CS2}/(k_{CR} - k_e) + k_r k_{CS1}/(k_{CR} - k_e)(k_{CS1} - k_e)]$, $A_2 = k_r k_{CS1}/(k_{CS1} - k_e)(k_{CS1} - k_{CR})]$, $A_3 = [k_r k_{CS1}/(k_{CS1} - k_e)(k_{CR} - k_{CS1}) - k_{CS2}/(k_{CR} - k_e) - k_r k_{CS1}/(k_{CR} - k_e)(k_{CS1} - k_e)]$. The experimental temperature-dependent transient absorption dynamics probed at 658 nm were reanalyzed with Eq. (26); this model is depicted in Fig. 19, which highlights the temperature-dependent values determined for S_1 manifold vibrational relaxation (k_r), CS from the vibronically equilibrated singlet excited state (k_{CS1}), and CS from the vibrationally unrelaxed **2a-Zn** S_1 state (k_{CS2}). This analysis predicts that the vibronic relaxation component (k_r) is ultrafast ($k_r > 1\ ps^{-1}$) at 310 K, and gradually decreases with decreasing temperature, until ~120 K, where it remains near constant at ~0.2 ps^{-1}. The evaluated k_{CS2} rate constant at temperatures between 310 and 180 K mirrored the magnitudes determined for k_r in this model. At temperatures below 180 K, k_{CS2} exceeds k_r and gradually increases until it reaches its maximal values of ~1.8 ps^{-1} at 100 K. It is important to note that this refined analysis (Eq. (26)) will not model well scenarios where either k_r or k_{CS2} approach zero (e.g., Fig. 18b); hence, k_{CS2} values determined at temperatures higher than 180 K and k_r values determined at temperatures lower than 100 K will express large associated errors. Fig. 19 shows clearly the distinctive temperature dependences of these three components. The temperature dependence of the S_1 manifold vibrational relaxation rate constant of the initially prepared **^{1}2a-Zn*** state is noteworthy, given the facts that it plays a highly unusual but key role in determining the temperature-dependent ET dynamics, and the fact that the k_r magnitude determined at 310 K mirrors that evaluated independently for electronically excited (porphinato)zinc(II) complexes [292–297].

With this refined model, the electronic coupling matrix element (H_{DA}) for the CS2 process was recalculated, and determined to be

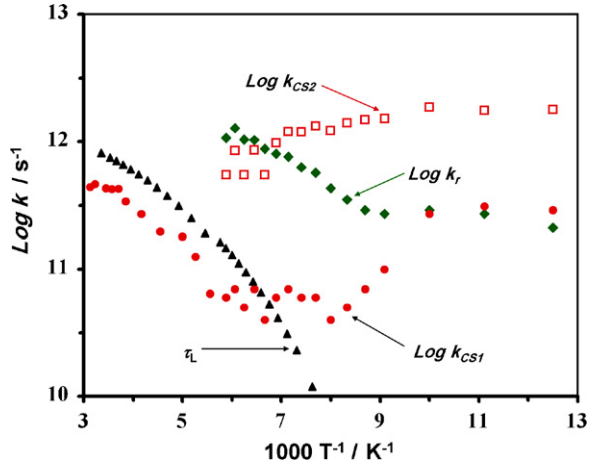

Fig. 19. Temperature dependence of the photoinduced charge separation rate constants for vibrationally unrelaxed (red open squares, k_{CS2}) and relaxed (red circles, k_{CS1}) **2a-Zn** S_1 states. The temperature dependent S_1 manifold vibrational relaxation rate constants are shown as green diamonds; see Eq. (26). The temperature dependent solvent longitudinal relaxation rate constants (τ_L^{-1}) for 2-MTHF are depicted as black triangles [152].

100 cm^{-1}. It is interesting that this H_{DA} value is more than a factor of two larger than that determined using an analysis that did not consider a vibrationally unrelaxed **2a-Zn** S_1-excited state. The Marcus model could not reproduce the temperature independent experimental CS component that became more prominent with increased reaction free energy, due mainly to the revival of the activation barrier manifest in the Marcus inverted region. The extent to which vibrationally relaxed and vibrationally unrelaxed excited-states feature disparate donor–acceptor electronic coupling has not been previously interrogated, due to the fact that systems that manifest two such measurable rate processes are extremely limited.

5. The distance dependence of electronic coupling

The complex temperature dependence of CS dynamics in **2a-Zn** complex clearly shows that the analysis of ET dynamics in these cofacially compressed, π-stacked porphyrin–bridge–quinone systems is not necessarily straightforward. Determinations of the magnitude of the electronic coupling matrix element in these systems depend critically on the mechanistic nature of the ET reaction; while such computations are uncomplicated for non adiabatic or super-exchange pathways, adiabatic or charge-hopping mechanisms cannot be analyzed within the context of the conventional Marcus or QM rate expressions. In Section 3, we raised the issue concerning the apparent adiabatic nature of the **1a-Zn** CS reaction, and noted that the evaluated electronic coupling for this process can thus not be incorporated in an analysis of distance dependence of the electronic coupling within the broader family of these π-stacked porphyrin–bridge–quinone structures. For the **1a-Zn** CR reaction, note that a computation based on QM ET rate equation gives an electronic coupling matrix element of ~85 cm^{-1} in CH_2Cl_2 solvent at ambient temperature; other means of probing the **1a-Zn** CR reaction, however, provide significantly different values for the magnitude of electronic coupling characteristic of the **1a-Zn** CS state. These analyses, summarized below, suggest substantial electronic coupling for the **1a-Zn** CR reaction, and indicate that like **1a-Zn** CS, this process is adiabatic.

5.1. Probing the magnitude of D–A electronic coupling in *1a-Zn* ground and charge-separated states

5.1.1. Direct charge transfer in *1a-Zn*

The properties of the adiabatic ground (ψ_G) and CS states (ψ_{CS}) can be described by the admixtures of the diabatic neutral (ψ_0) and charge-separated (ψ_1) wavefunctions [299–304] assuming the overlap integral $\left(\left\langle \psi_0 \psi_1 \right\rangle\right)$ is neglected.

$$\Psi_G = c_0\psi_0 + c_1\psi_1 \tag{27}$$

$$\Psi_{CT} = c_0\psi_1 - c_1\psi_0 \tag{28}$$

The contribution of the charge-separated wave function, ψ_1, in the unperturbed ground-state wavefunction, can be estimated from the electronic coupling matrix element H_{DA} by the relation $|c_0c_1| \approx |H_{DA}/\Delta E|$, where ΔE is the ground-to-CS state energy gap. Although it is assumed to be valid in the weak coupling limit ($|c_0| \approx 1$, $|c_0c_1| \approx |H_{DA}/\Delta E|$), Creutz, Newton, and Sutin verified that it is exact for any orthonormal two-state model; for example, at $|c_0c_1| \approx 0$ and when $|c_0c_1|$ has its maximum value of 1/2 [299–304].

Mulliken and Hush relate the strength of the transition dipole moment of a charge transfer band to the magnitude of the off-diagonal electronic coupling between the ψ_0 and ψ_1 states, which provides an approach to determine the magnitude of the electronic coupling directly from strongly coupled D–A systems that possess a charge transfer absorption band.

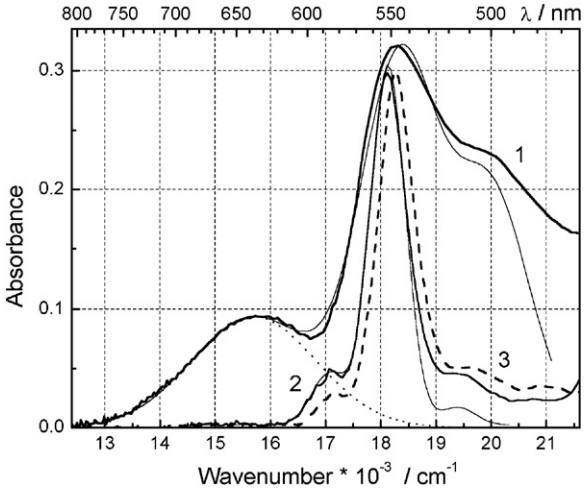

Fig. 20. Steady-state absorption spectra recorded for: **1a-Zn** (1), **1M-Zn** (2), and **2a-Zn** (3, dashed line) in CH_2Cl_2 solvent. Spectral fitting using a multi-peak Gaussian function for **1a-Zn** and **1M-Zn** are shown by thin lines. The component of the fit corresponding to the CT band **1a-Zn** is highlighted by the dotted line [151].

$$H_{DA} = 2.06 \times 10^{-2} \frac{\sqrt{\nu_{max}\varepsilon_{max}\Delta\nu_{fwhm}}}{R_{DA}} \tag{29}$$

Here ν_{max} and $\Delta\nu_{fwhm}$ are the CT band maximum frequency and width in wave numbers, ε_{max} is the extinction coefficient at the band maximum in $(M\,cm)^{-1}$, and R_{DA} is the D–A separation distance in Å [305–307].

The electronic absorption spectra obtained for **2a-Zn** and **3a-Zn** resemble that for the **TPPZn** benchmark, suggesting that the cofacially π-stacked phenyl and quinonyl moieties do not perturb significantly the porphyrin/quinone ground- and excited-state wavefunctions (Fig. 20). In contrast, note that the optical spectrum of **1a-Zn** is perturbed strongly relative to those observed for conventional PZn compounds. As the spectrum of the **1M-Zn** (Fig. 20) is similar to that of **TPPZn** and **2a-Zn**, the unique spectral features observed in the **1a-Zn** spectrum must derive from a porphyrin–quinone charge resonance interaction. **1a-Zn** exhibits Q(2,0) and Q(1,0) transitions at wavelengths near where the analogous absorptions occur in the **TPPZn** (Fig. 20) spectrum (~510 and 550 nm), though the bands are significantly broader in **1a-Zn**. Interestingly, a new band centered at 635 nm, not present in a conventional **PZn** optical spectrum, is evident for **1a-Zn**, with an absorption envelope even broader than those in the **1a-Zn** spectrum centered at 510 and 550 nm. This new band at 635 nm is assigned to a CT transition; this CT state possesses significant quinonyl π^* and porphyrin Q-state character, and is red-shifted ~2000 cm^{-1} from conventional PZn Q-band absorptions. From the Mulliken–Hush relation (Eq. (29)), the electronic coupling between the neutral ground state and the CT state in **1a-Zn** is estimated to be 2330 cm^{-1} in $CDCl_3$ solvent (ν_{max} = 14,980 cm^{-1}, $\Delta\nu_{fwhm}$ = 2980 cm^{-1}, and $\varepsilon_{max} = 2.6 \times 10^3$ $cm^{-1}\,M^{-1}$) [299–304]. This value is surprisingly similar to that estimated to exist between the **1a-Zn** locally excited and CT states, based on an evaluated time constant for charge separation of ~20 fs [149].

The higher lying Q-states of **1a-Zn** mix less effectively with the quinonyl LUMO; this interaction is nonetheless substantial, and results in broadening of these bands with respect to their **TPPZn** benchmarks. To quantify the extent to which these **1a-Zn** absorptions bands are broadened, the **1a-Zn** and **1M-Zn** spectra were simplex fit to a multi-peak Gaussian function. The Q-state region of **1b-Zn** can be fit by three Gaussian functions having identical

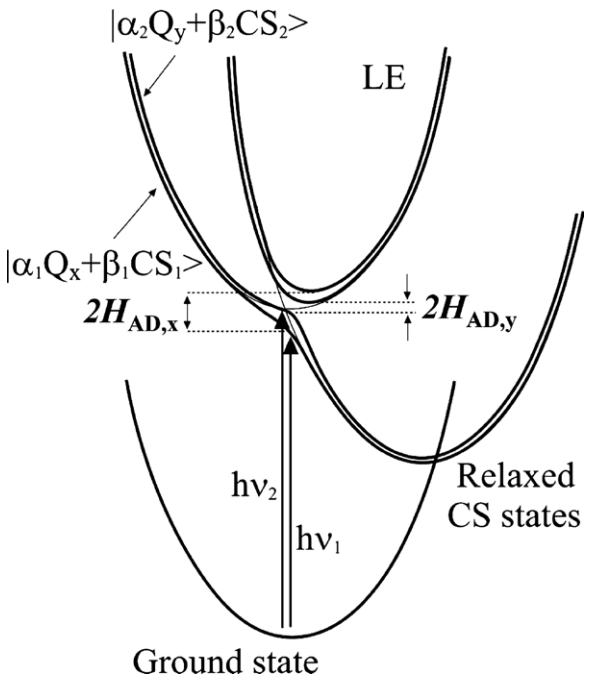

Fig. 21. Potential energy surfaces describing the ground, local excited, and CS states for **1a-Zn**. Diabatic states are presented as thin lines while adiabatic states are shown as thick lines. Vertical excitations are indicated by arrows [308].

spectral width (755 cm^{-1}, FWHM). Deconvolution of the **1a-Zn** spectrum requires at a minimum Gaussian functions of different spectral widths to fit the absorption envelopes centered at 510, 550, and 630 nm, the FWHM of these Gaussian peak functions are 2640, 1640, and 1640 cm^{-1}, respectively. An energy level diagram consistent with these **1a-Zn** spectral features is shown in Fig. 21. Diabatic potential energy surfaces for locally excited (LE) and CS states of **1a-Zn** are shown as thin lines [(only one line in drawn for both degenerate Q_x and Q_y states)]. Note that the CS reaction is described by an adiabatic surface (*vide infra*). The ratio of the LE (denoted as Q_x) vs. CS state changes along the PE surface. It is unclear what this ratio corresponds to in the Frank–Condon (FC) region. The larger contribution of the CS state effects a greater reorganization energy of this transition and a broader spectrum, relative to a classic porphyrin LE Q-state transition. If the interaction is so large that the FC transition gives rise to an excited state with significant D–A charge separation, the CS reaction can be treated as instantaneous and transition can then be termed as CT in nature. At weaker D–A electronic interaction, when the FC state is essentially unpolarized, and formation of a LE state precedes the CS reaction. A direct CS reaction is treated as a motion along the adiabatic potential surface toward its minimum, which represents the largest charge separation possible in this molecular system. The CS rate constant in this case can be estimated from the broadening of the CT transition.

The fact that the **1a-Zn** bands centered at 510 and 550 nm resemble the analogous transitions observed in the **1M-Zn** (Fig. 20) optical spectrum, suggest that these optical transitions form essentially unpolarized, porphyrin-localized π–π^* states. The spectral broadening of these states are attributed to their short lifetime; an excited state lifetime estimated from the additional broadening of these **1a-Zn** bands ($\Delta E \sim 1000\ cm^{-1}$) relative to corresponding benchmark (porphinato)zinc Q(2,0) and Q(1,0) transitions, via the uncertainty principle: $\Delta\tau \sim 0.4/\Delta E$ provides a τ_{CS} value of 13 fs, which corresponds to the characteristic time of the CS reaction, when **1a-Zn** is excited at 510 or 550 nm [308]. Note also that the magnitude of τ_{CS} evaluated in this manner is similar to that estimated for **1a-Zn** from pump–robe transient absorption spectral

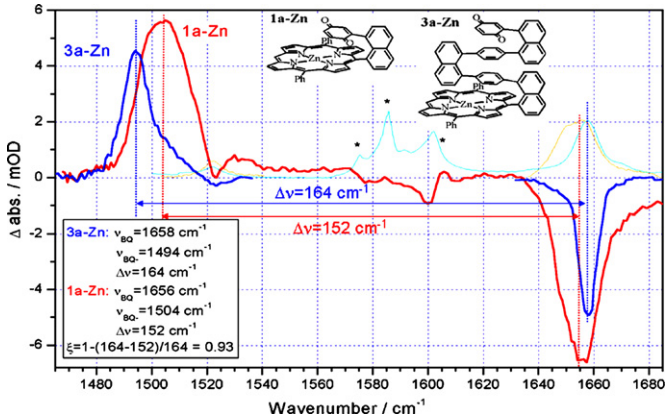

Fig. 22. Transient IR spectra of **1a-Zn** and **3a-Zn**. Time delays for **1a-Zn** and **3a-Zn**. Transient spectra are 0.6 and 5.0 ps, respectively. Experimental conditions: λ_{ex} = 580 nm, solvent = 99:1 $CDCl_3$:pyridine-d_5, $T = 23 \pm 1\ ^\circ C$ [151].

data obtained in CH_2Cl_2 solvent for a 557 nm excitation wavelength [149].

5.1.2. *Evaluating **1a-Zn** electronic coupling utilizing vis-pump/IR-probe spectroscopic methods*

In addition to the classic CT absorption band analysis to estimate the magnitude of electronic coupling, we have utilized a new approach that relies on femtosecond visible pump/mid-IR probe spectroscopy to assess directly the extent the degree of ground- and excited-state CT that exists in the **1a-Zn** and **3a-Zn** systems. Fig. 22 displays the quinonyl carbonyl antisymmetric stretching mode frequency domain of **1a-Zn** and **3a-Zn**; note that the transient IR spectra show that these modes shift to significantly lower energy relative to the ground state frequencies in the respective charge-separated (CS) states of these complexes. These frequency shifts reflect the decreased force constants for these modes in the CS state, tracking the augmented A-localized electronic charge in this state relative to the ground state.

The quinonyl carbonyl mode acceptor frequency depends on the vibrational force constant (k), $\nu_{CO} = \sqrt{k/m_r}/2\pi c$. The force constant in the ground and CS states changes with a weighted average contribution of the charge resonant state. If the frequency change, $\Delta\nu_A$, is small relative to the ground-state frequency ($\Delta\nu_A \ll \nu_A$; $\Delta\nu_A = \nu_A - \nu_{A^-}$) and the D–A interaction is weak ($\delta \ll \Delta\nu_A$, where δ is the frequency change in the ground state due to the contribution of the charge-resonance state), the magnitude of δ can be computed from the value of C_2^2 ($C_2 = |c_0 c_1|$) [10,151,305]: $\delta \cong \Delta\nu_A^\circ C_2^2$, where $\Delta\nu_A^\circ = \Delta\nu_A^\circ - \Delta\nu_A^{\circ -}$, and $\Delta\nu_A^\circ$ and $\Delta\nu_A^{\circ -}$ are ground- and CS-state Q vibrational frequencies that lack contributions, respectively, from the ψ_1 and ψ_0 wave functions (Eqs. (27) and (28)). This experimentally measured relative frequency shift $\xi(\xi = \Delta\nu_A^\circ - \Delta\nu_A)/\Delta\nu_A^\circ)$ can be used to estimate the extent to which the CT wave function contributes to ψ_G [151].

The experimentally determined charge-resonance contribution to the ground state ($\xi/2$) of **1a-Zn** is 3.57% (Fig. 22). The charge-resonance contribution (C_2^2) to ψ_G can also be estimated from the electronic coupling matrix element (H_{DA}) because $C_2 = |c_0 c_1|$, which is again $|H_{DA}/\Delta E|$[151].

$$H_{DA} \approx \Delta E \sqrt{\left(1 - \frac{\xi}{2}\right)\frac{\xi}{2}} \tag{30}$$

Recall that a Mulliken–Hush analysis of the **1a-Zn** CT band (Fig. 20) gave $H_{DA} = 2064\ cm^{-1}$; this analysis that exploits transient spectral data obtained from vis-pump/IR-probe spectroscopic data provides

Table 2
Electronic couplings for (**1**–**3**)**a-Zn** structures [127].

	PM3 optimized			DFT optimized		
	D–A distance[a] (Å)	CS, H_{DA} (eV)	CR, H_{DA} (eV)	D–A distance[a] (Å)	CS, H_{DA} (eV)	CR, H_{DA} (eV)
1a-Zn	3.65	2.27×10^{-1}	2.18×10^{-1}	3.37	3.82×10^{-1}	3.23×10^{-1}
2a-Zn	6.88	4.60×10^{-2}	4.64×10^{-2}	7.11	9.20×10^{-2}	9.25×10^{-2}
3a-Zn	10.54	3.14×10^{-2}	3.14×10^{-2}	10.62	4.11×10^{-2}	4.11×10^{-2}

[a] D–A distance is the porphyrin plane-to-quinonyl centroid distances for computationally determined structures [315].

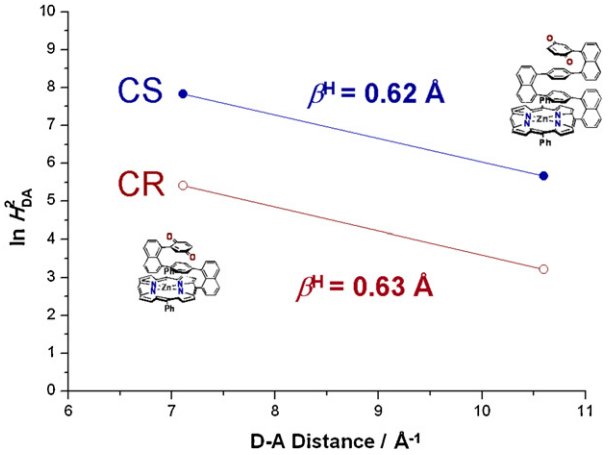

Fig. 23. Distance dependence of the CS and CR rate constants for (**2**–**3**)**a-Zn** in methylene chloride at 23 ± 1 °C.

$H_{DA} = 2457\,cm^{-1}$ ($\Delta E = 13{,}000\,cm^{-1}$ and a $\xi/2 = C_2^2 = 0.0357$), a remarkably similar value.

This method further affords a more accurate measure of the degree of CT relative to methods [299–304] that rely on a ground-state frequency shift alone, as determination of $\Delta\nu_A$ largely factors out frequency shifts that derive from the local electrostatic environment. This approach may thus find particular utility when CT transitions either overlap strongly with other bands or possess low oscillator strength.

5.2. The distance dependence of electronic coupling in the nonadiabatic ET regime

Given the discussion above, we see that an analysis of distance dependence of electronic coupling in (**1**–**3**)**a-Zn**, is only appropriate for (**2**–**3**)**a-Zn**, as the CS and CR reactions of **1a-Zn** are adiabatic in nature. This is illustrated in Fig. 23, which shows $\beta^H = 0.62^{-1}$ for CS and for $\beta^H = 0.63^{-1}$ CR; these values are smaller than that determined for the DNA hairpin structures interrogated by Lewis and Wasielewski ($\beta^H = 0.77^{-1}$ for distance dependence of electronic coupling). If we consider the phenomenological ET rate constants, (**1**–**3**)**a-Zn** β values ($\beta = 0.43$ for CS and $\beta = \sim 0.35$ for CR) are similar in magnitude to that reported for the paraphenylene-bridged zinc-ferric hybrid diporphyrins of Maruyama and Mataga [252] and McLendon ($\beta = 0.4$) [70]. It should be noted that the tunneling energy gap in (**2**–**3**)**a-Zn** is ~2 eV larger than that for double-stranded DNA, based on the electron injection free energy analysis discussed in section 3. While the k_{ET} data that lie in the nonadiabatic regime are more limited in these D-Sp-A assemblies, it is nonetheless noteworthy that the weaker distance dependence in (**2**–**3**)**a-Zn** relative to DNA-based ET assemblies indicates that at sub van der Waals contact distances, compressed π-stacked phenylenes provide stronger D–A electronic coupling than do the significantly more conjugated DNA nucleotides stacked at the van der Waals distance.

6. Computationally determined electronic couplings in (1–3)a-Zn

6.1. GMH calculations of electronic coupling for (*1*–*3*)*a-Zn*

Newton and Cave introduced a generalized Mulliken–Hush (GMH) approach [10,309,310] to compute donor-acceptor interactions, based on the pioneering models of Mulliken and Hush [306,311]. This approach can be used to calculate H_{DA} for both ground- and excited-state electron-transfer reactions [312].

The two-state generalized Mulliken–Hush approximation computes H_{DA} as [10,309,310,312]:

$$H_{DA} = \frac{\mu_{12}\Delta E_{12}}{\Delta\mu_{12}^D} = \frac{\mu_{12}\Delta E_{12}}{\sqrt{\Delta\mu_{12}^2 + 4\mu_{12}^2}} \quad (31)$$

where μ_{12} is the transition dipole moment connecting the two adiabatic states in the charge transition, $\Delta\mu_{12}$ is the difference in adiabatic state dipole moments, $\Delta\mu_{12}^D$ is the difference in diabatic state dipole moments, and ΔE_{12} is the energy difference between the initial and final adiabatic states. For simplicity, we used a three-state model. The three diabatic states are the donor ground state (GS), a donor locally excited (LE) state, and a charge-transfer (CT) state. For the charge separation process, the LE and CT states were described with a two-state GMH model; for charge recombination, the CT and GS states were used. Electronic coupling was obtained from configuration interaction (CI) calculations using the INDO/S method of Zerner and co-workers [313,314].

We calculated electronic coupling values for both PM3 and DFT optimized geometries (Table 2). Using a PM-3 optimized geometry, **1a-Zn** was computed to possess strong electronic coupling (~0.23 eV) for both its photoinduced CS and thermal CR reactions, consistent with the above discussion that strongly suggests that these **1a-Zn** ET reactions lie in the adiabatic regime. Excluding **1a-Zn** from the analysis, the computed distance dependence, β, for structures (**2**–**3**)**a-Zn** is 0.21 $Å^{-1}$ for both the CS and CR processes, a weaker value than that determined experimentally. Note that the couplings calculated from DFT-based structures give rise to more steep distance of the electronic coupling ($\beta = 0.46\,Å^{-1}$) more closely in line with experiment.

From a structural perspective, this result is consistent with the fact that DFT optimization describes the π-stacked geometry more accurately than the PM3 method; note that the porphyryl-phenyl interplanar separation and the phenyl/quinonyl tilt angles determined for DFT-optimized structures more closely resemble those of the experimentally determined solution phase structure (see Section 2).

6.2. Coupling calculations for partial structures

To understand the influence of the bridge on the electron tunneling interactions, we calculated H_{DA} for partial structures based on both PM3- and DFT-optimized (**2**–**3**)**a-Zn** geometries. Fig. 24 shows the partial structures that were examined; note that deleted fractions of complete D–A systems are replaced with an H atom). Tables 3 and 4 show the computed couplings. The detailed calculations on **2a-Zn** and **3a-Zn** indicate that the phenyl rings between

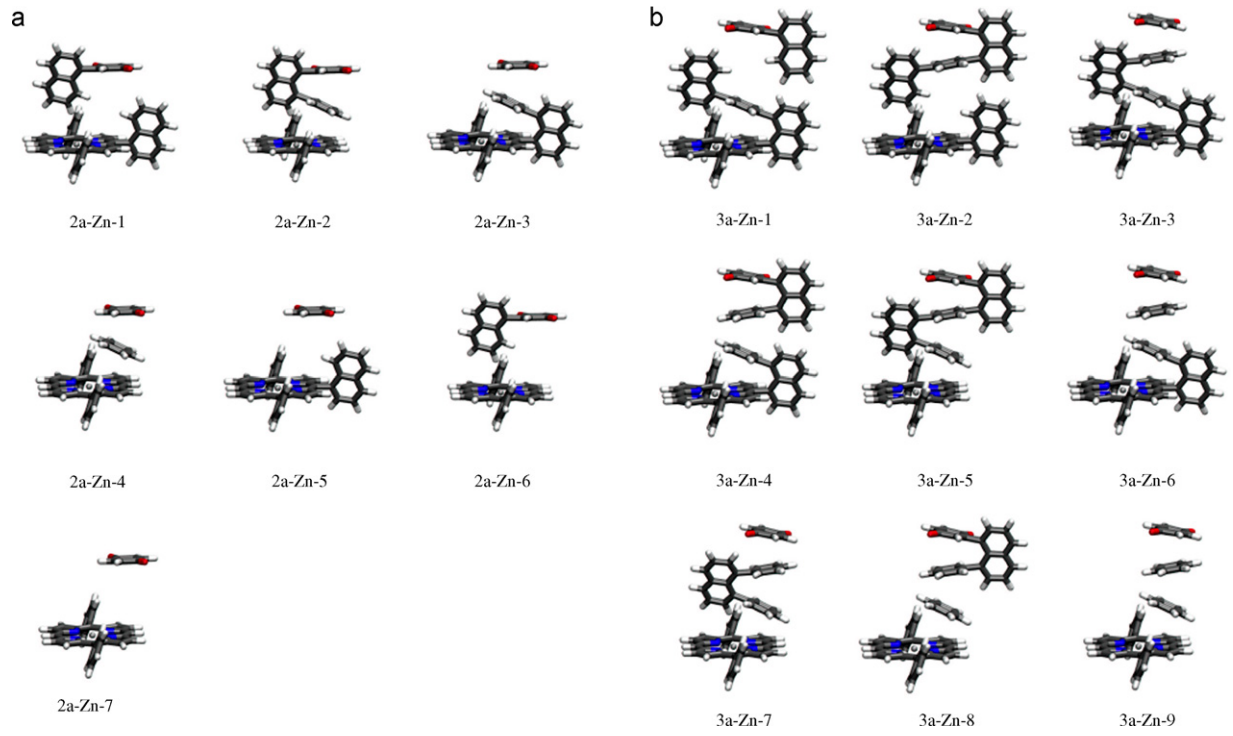

Fig. 24. Partial structures used to analyze electronic coupling in **2a-Zn** (a) and **3a-Zn** (b) [127].

Table 3
H_{DA} (eV) for partial **2a-Zn** structures [127].

	PM3 optimized		DFT optimized	
	CS	CR	CS	CR
2a-Zn-1	1.32×10^{-3}	1.32×10^{-3}	1.58×10^{-3}	1.58×10^{-3}
2a-Zn-2	3.12×10^{-2}	3.13×10^{-2}	4.04×10^{-2}	4.07×10^{-2}
2a-Zn-3	2.10×10^{-2}	2.11×10^{-2}	5.78×10^{-2}	5.82×10^{-2}
2a-Zn-4	1.21×10^{-3}	1.21×10^{-3}	4.21×10^{-2}	4.23×10^{-3}
2a-Zn-5	9.89×10^{-4}	9.91×10^{-4}	1.07×10^{-3}	1.08×10^{-3}
2a-Zn-6	1.50×10^{-4}	1.50×10^{-4}	1.11×10^{-4}	1.11×10^{-4}
2a-Zn-7	1.44×10^{-5}	1.44×10^{-5}	2.33×10^{-5}	2.33×10^{-5}

donor and acceptor dominate the coupling mediation. For **2a-Zn**, the coupling drops by a factor of 35–50 when the phenyl ring is removed (structure **2a-Zn-1**; see Fig. 24). However, removing either one of the two naphthyl rings decreases the coupling only by about a factor of 2 (structures **2a-Zn-2** and **2a-Zn-3**; see Fig. 24). A similar trend was found in **3a-Zn**. Removing the phenyl ring adjacent to the quinonyl ring (structure **3a-Zn-1**; see Fig. 24) decreases the coupling by a factor of 35–55. Removing the phenyl ring adjacent to the porphyryl ring decreases the coupling by a factor of 70–90 (structure **3a-Zn-2**; see Fig. 24). However, when one of the naphthyl rings is removed, the coupling only changes by a factor of 1.5 (structures **3a-Zn-3**, **3a-Zn-4**, and **3a-Zn-5**; see Fig. 24). The large variation in coupling upon removing a phenyl bridge unit confirms that the π-stack, rather than the "pillars", dominates the electronic propagation through the bridge in (**1**–**3**)**a-Zn**.

Table 4
H_{DA} (eV) for partial **3a-Zn** structures.

	PM3 optimized		DFT optimized	
	CS	CR	CS	CR
3a-Zn-1	9.16×10^{-4}	9.19×10^{-4}	7.42×10^{-4}	7.61×10^{-4}
1a-Zn-2	4.62×10^{-4}	4.60×10^{-4}	4.73×10^{-4}	4.83×10^{-4}
3a-Zn-3	2.13×10^{-2}	2.13×10^{-2}	3.40×10^{-2}	3.41×10^{-2}
3a-Zn-4	1.66×10^{-2}	1.66×10^{-2}	3.44×10^{-2}	3.44×10^{-2}
3a-Zn-5	1.48×10^{-2}	1.48×10^{-2}	2.72×10^{-2}	2.73×10^{-2}
3a-Zn-6	3.02×10^{-3}	2.97×10^{-3}	3.13×10^{-2}	3.14×10^{-2}
3a-Zn-7	1.48×10^{-2}	1.48×10^{-2}	2.99×10^{-2}	3.00×10^{-2}
3a-Zn-8	1.18×10^{-2}	1.18×10^{-2}	3.00×10^{-2}	3.02×10^{-2}
3a-Zn-9	7.87×10^{-3}	7.87×10^{-3}	3.35×10^{-2}	3.36×10^{-2}

7. Concluding remarks

A series of uniquely rigid, π-stacked porphyrin–spacer–quinone ET assemblies, [5-[8′-(2″,5″-benzoquinonyl)-1′-naphthyl]-10,20-diphenylporphinato]zinc(II) (**1a-Zn**), [5-[8′-(4″-[8‴-(2‴,5‴-benzoquinonyl)-1‴-naphthyl]-1″-phenyl)-1′-naphthyl]-10,20-diphenylporphinato]zinc(II) (**2a-Zn**), and [5-(8′-[4″-(8‴-[4⁗-(8⁗⁗-[2⁗⁗,5⁗⁗-benzoquinonyl]-1⁗⁗-naphthyl)-1‴-phenyl]-1″-naphthyl)-1″-phenyl]-1′-naphthyl)-10,20-diphenylporphinato]zinc(II) (**3a-Zn**), have been defined in which the interplanar distances between D, bridge, and A aromatic units are less than the sums of their respective van der Waals radii. The 1,8-diarylnaphthalene pillaring motif, coupled with the presence of a basal porphyryl moiety, ensures significant molecular rigidity in these D–Sp–A systems and limits conformational heterogeneity in solution. The 1D ^{1}H NMR and 2D NMR data of these compounds show that: (i) the structures constrain nuclei to reside in unusual and diverse local magnetic environments, and (ii) the close contacts afforded by a sub van der Waals interplanar separation of D, Sp, and A give rise to a comprehensive set of structurally significant NOE signatures that can be used as constraints in quantitative structural calculations. Examination of such data using *ab initio* SA analysis shows that compound **2a** constitutes an unusual example for which these analytical tools unequivocally determine a single unique structure in solution.

The electron-transfer (ET) dynamics of these structures were investigated using pump-probe transient absorption spectroscopic methods. Analyses of these data show that the phenomenological ET distance dependence (β) for both the CS and CR reactions in these systems is soft ($\beta_{CS} = 0.43$ Å^{-1}; $\beta_{CR} = 0.35 \pm 0.16$ Å^{-1}) indicating that simple aromatic building blocks such as benzene, which are characterized by highly stabilized filled molecular orbitals and

large HOMO–LUMO gaps, can provide substantial D–A electronic coupling when organized within a π-stacked structural motif that features a modest degree of arene–arene interplanar compression.

Temperature-dependent ET dynamical studies of both the photoinduced CS and thermal CR reactions of **2a-Zn** in 2-MTHF solvent demonstrated: (1) a dominant photoinduced charge-separation pathway at low temperature ($T < 150$ K) that originates from a vibrationally unrelaxed S_1 state. These dynamics derive from the facts that (i) the initially prepared S_1 state by the laser excitation features ~0.17 eV of excess energy and a H_{DA} value significantly larger than that for the relaxed S_1 state and (ii) the S_1 manifold vibrational relaxation rate constant (k_r) decreases with decreasing temperature. (2) An unusual solvent-controlled adiabatic ET in moderately polar 2-MTHF solvent (ε_S ~14 at 150 K, the temperature at which the degree of solvent-controlled adiabaticity is maximized). (3) A transition from the solvent-controlled adiabatic regime to one where charge separation is governed by nuclear tunneling within an upper vibronic state of the S_1 manifold. Over this mechanistic transition, the CS rate constants increased by approximately 1 order of magnitude, driven in part by the reaction energetics, which showed a smooth change from normal-to-inverted region with decreasing temperature. (4) A rare example of a system where temperature-dependent photoinduced charge-separation (CS) dynamics from vibrationally relaxed and unrelaxed S_1 states can be differentiated. (5) A temperature-dependent mechanistic transition of photoinduced CS from the nonadiabatic to the solvent-controlled adiabatic regime, followed by a second temperature-dependent mechanistic evolution where CS becomes decoupled from solvent dynamics and is determined by the extent to which the vibrationally unrelaxed S_1 state is populated.

Additional studies that evaluate the electronic coupling utilized both CT band analysis and vis-pump/IR probe spectroscopy. This work showed that the electronic coupling between the ground state and the CS state of **1a-Zn** exceeds 2000 cm^{-1}, consistent with the conclusion that the CS and CR reactions of **1a-Zn** are adiabatic in nature. Analysis of the nonadiabatic ET dynamics characteristic of **2a-Zn** and **3a-Zn** provides distance dependences for the electronic coupling corresponding to $\beta^H = 0.62$ $Å^{-1}$ for CS and $\beta^H = 0.63$ $Å^{-1}$ for CR.

These experimental results are consistent with expectations derived from theory. GMH computational results indicate that the electronic coupling is strongly dependent on the extent of ring compression in these rigid, π-stacked porphyrin–bridge–quinone systems, underscoring the unusual structural factors in (**1**–**3**)**a-Zn** that give rise to substantial D–A coupling. While GMH analysis predicted the distance dependences of electronic coupling in (**1**–**3**)**a-Zn** as slightly weaker than those determined from experiment, it verified that the aromatic ring systems held at sub-van der Waals contact provided the crucial tunneling mediation and substantial electronic coupling.

Acknowledgements

This work was supported by a grant from the Department of Energy (DE-SC0001517). The authors thank the NSF MRSEC (DMR0520020), NSF NSEC (DMR04-25780), the Office of Naval Research (N00014-06-1-0360), and DOE EFRC (P353-0127) for infrastructural support.

References

[1] N.S. Hush, Coord. Chem. Rev. 64 (1985) 135.
[2] S.L. Mayo, W.R. Ellis, R.J. Crutchley, H.B. Gray, Science 233 (1986) 948.
[3] G.J. Kavarnos, N.J. Turro, Chem. Rev. 86 (1986) 401.
[4] G.L. Closs, J.R. Miller, Science 240 (1988) 440.
[5] G. McLendon, Acc. Chem. Res. 21 (1988) 160.
[6] M. Plato, K. Mobius, M.E. Michel-Beyerle, M. Bixon, J. Jortner, J. Am. Chem. Soc. 110 (1988) 7279.
[7] S.S. Isied, M.Y. Ogawa, J.F. Wishart, Chem. Rev. 92 (1992) 381.
[8] M.R. Wasielewski, Chem. Rev. 92 (1992) 435.
[9] J.R. Winkler, H.B. Gray, Chem. Rev. 92 (1992) 369.
[10] C. Creutz, M.D. Newton, N. Sutin, J. Photochem. Phtobiol. A 82 (1994) 47.
[11] M.N. Paddon-Row, Acc. Chem. Res. 27 (1994) 18.
[12] J.P. Sauvage, J.P. Collin, J.C. Chambron, S. Guillerez, C. Coudret, V. Balzani, F. Barigelletti, L. Decola, L. Flamigni, Chem. Rev. 94 (1994) 993.
[13] V. Balzani, A. Juris, M. Venturi, S. Campagna, S. Serroni, Chem. Rev. 96 (1996) 759.
[14] P.F. Barbara, T.J. Meyer, M.A. Ratner, J. Phys. Chem. 100 (1996) 13148.
[15] N.C. Greenham, X.G. Peng, A.P. Alivisatos, Phys. Rev. B 54 (1996) 17628.
[16] H. Imahori, Y. Sakata, Adv. Mater. 9 (1997) 537.
[17] P.Y. Chen, T.J. Meyer, Chem. Rev. 98 (1998) 1439.
[18] R.I. Cukier, D.G. Nocera, Annu. Rev. Phys. Chem. 49 (1998) 337.
[19] K.E. Erkkila, D.T. Odom, J.K. Barton, Chem. Rev. 99 (1999) 2777.
[20] C.C. Page, C.C. Moser, X.X. Chen, P.L. Dutton, Nature 402 (1999) 47.
[21] J.W. Verhoeven, Electron Transfer-from Isolated Molecules to Biomolecules Pt 1, vol. 106, 1999, p. 603.
[22] B. Giese, Acc. Chem. Res. 33 (2000) 631.
[23] G.B. Schuster, Acc. Chem. Res. 33 (2000) 253.
[24] K.D. Demadis, C.M. Hartshorn, T.J. Meyer, Chem. Rev. 101 (2001) 2655.
[25] D. Gust, T.A. Moore, A.L. Moore, Acc. Chem. Res. 34 (2001) 40.
[26] F.D. Lewis, R.L. Letsinger, M.R. Wasielewski, Acc. Chem. Res. 34 (2001) 159.
[27] A. Nitzan, Annu. Rev. Phys. Chem. 52 (2001) 681.
[28] L.C. Sun, L. Hammarstrom, B. Akermark, S. Styring, Chem. Soc. Rev. 30 (2001) 36.
[29] B.S. Brunschwig, C. Creutz, N. Sutin, Chem. Soc. Rev. 31 (2002) 168.
[30] D.M. Guldi, Chem. Soc. Rev. 31 (2002) 22.
[31] D. Holten, D.F. Bocian, J.S. Lindsey, Acc. Chem. Res. 35 (2002) 57.
[32] P.V. Kamat, J. Phys. Chem. B 106 (2002) 7729.
[33] D.M. Adams, L. Brus, C.E.D. Chidsey, S. Creager, C. Creutz, C.R. Kagan, P.V. Kamat, M. Lieberman, S. Lindsay, R.A. Marcus, R.M. Metzger, M.E. Michel-Beyerle, J.R. Miller, M.D. Newton, D.R. Rolison, O. Sankey, K.S. Schanze, J. Yardley, X.Y. Zhu, J. Phys. Chem. B 107 (2003) 6668.
[34] M. Gratzel, J. Photochem. Photobiol. C 4 (2003) 145.
[35] A. Nitzan, M.A. Ratner, Science 300 (2003) 1384.
[36] J.L. Bredas, D. Beljonne, V. Coropceanu, J. Cornil, Chem. Rev. 104 (2004) 4971.
[37] D. Kim, A. Osuka, Acc. Chem. Res. 37 (2004) 735.
[38] F. Wurthner, Chem. Commun. (2004) 1564.
[39] L. Venkataraman, J.E. Klare, C. Nuckolls, M.S. Hybertsen, M.L. Steigerwald, Nature 442 (2006) 904.
[40] A.C. Benniston, A. Harriman, Chem. Soc. Rev. 35 (2006) 169.
[41] V. Coropceanu, J. Cornil, D.A. da Silva, Y. Olivier, R. Silbey, J.L. Bredas, Chem. Rev. 107 (2007) 926.
[42] B. Albinsson, J. Martensson, J. Photochem. Photobiol. C 9 (2008) 138.
[43] Z.W. Lin, C.M. Lawrence, D.Q. Xiao, V.V. Kireev, S.S. Skourtis, J.L. Sessler, D.N. Beratan, I.V. Rubtsov, J. Am. Chem. Soc. 131 (2009) 18060.
[44] B. Farrow, P.V. Kamat, J. Am. Chem. Soc. 131 (2009) 11124.
[45] V.W. Manner, J.M. Mayer, J. Am. Chem. Soc. 131 (2009) 9874.
[46] J. Vura-Weis, S.H. Abdelwahed, R. Shukla, R. Rathore, M.A. Ratner, M.R. Wasielewski, Science 328 (2010) 1547.
[47] T. Honda, T. Nakanishi, K. Ohkubo, T. Kojima, S. Fukuzumi, J. Am. Chem. Soc. 132 (2010) 10155.
[48] A.P.S. Samuel, D.T. Co, C.L. Stern, M.R. Wasielewski, J. Am. Chem. Soc. 132 (2010) 8813.
[49] W.A. Tisdale, K.J. Williams, B.A. Timp, D.J. Norris, E.S. Aydil, X.Y. Zhu, Science 328 (2010) 1543.
[50] K. Kawai, H. Kodera, T. Majima, J. Am. Chem. Soc. 132 (2010) 627.
[51] Y.S. Nam, T. Shin, H. Park, A.P. Magyar, K. Choi, G. Fantner, K.A. Nelson, A.M. Belcher, J. Am. Chem. Soc. 132 (2010) 1462.
[52] P.A.M. Dirac, Proc. R. Soc. Lond. A 114 (1927) 243.
[53] R.A. Marcus, J. Chem. Phys. 24 (1956) 979.
[54] R.A. Marcus, J. Chem. Phys. 24 (1956) 966.
[55] V.G. Levich, Adv. Electrochem. Eng. 4 (1966) 249.
[56] R.R. Dogonadze, E.M. Kuznetsov, V.G. Levich, Electrochim. Acta 13 (1968) 1025.
[57] S. Efrima, M. Bixon, Chem. Phys. Lett. 25 (1974) 34.
[58] R.P. Van Duyne, R.S. Fisher, Chem. Phys. 5 (1974) 183.
[59] J. Jortner, J. Chem. Phys. 64 (1976) 4860.
[60] P. Siders, R.A. Marcus, J. Am. Chem. Soc. 103 (1981) 748.
[61] H.M. McConnell, J. Chem. Phys. 35 (1961) 508.
[62] D.N. Beratan, J.J. Hopfield, J. Am. Chem. Soc. 106 (1984) 1584.
[63] J.N. Onuchic, D.N. Beratan, J. Am. Chem. Soc. 109 (1987) 6771.
[64] K.D. Jordan, M.N. Paddon-Row, Chem. Rev. 92 (1992) 395.
[65] K. Huang, A. Rhys, Proc. R. Soc. Lond. A 204 (1950) 406.
[66] M. Bixon, J. Jortner, Adv. Chem. Phys. 106 (1999) 35.
[67] R.A. Marcus, N. Sutin, Biochim. Biophys. Acta: Rev. Bioenerg. 811 (1985) 265.
[68] F.D. Lewis, J.Q. Liu, W. Weigel, W. Rettig, I.V. Kurnikov, D.N. Beratan, Proc. Natl. Acad. Sci. U. S. A. 99 (2002) 12536.
[69] S. Strauch, G. McLendon, M. McGuire, T. Guarr, J. Phys. Chem. 87 (1983) 3579.
[70] A. Helms, D. Heiler, G. McLendon, J. Am. Chem. Soc. 114 (1992) 6227.
[71] L.H. Guo, J.S. Facci, G. McLendon, J. Phys. Chem. 99 (1995) 8458.
[72] B.S. Brunschwig, S. Ehrenson, N. Sutin, J. Am. Chem. Soc. 106 (1984) 6858.
[73] T.T.T. Li, M.J. Weaver, J. Am. Chem. Soc. 106 (1984) 6107.

[74] N.S. Hush, M.N. Paddon-Row, E. Cotsaris, H. Oevering, J.W. Verhoeven, M. Heppener, Chem. Phys. Lett. 117 (1985) 8.
[75] H. Oevering, M.N. Paddon-Row, M. Heppener, A.M. Oliver, E. Cotsaris, J.W. Verhoeven, N.S. Hush, J. Am. Chem. Soc. 109 (1987) 3258.
[76] M.N. Paddon-Row, J.W. Verhoeven, New J. Chem. 15 (1991) 107.
[77] M. Antolovich, P.J. Keyte, A.M. Oliver, M.N. Paddon-Row, J. Kroon, J.W. Verhoeven, S.A. Jonker, J.M. Warman, J. Phys. Chem. 95 (1991) 1933.
[78] K.D. Jordan, M.N. Paddon-Row, J. Phys. Chem. 96 (1992) 1188.
[79] J.M. Warman, K.J. Smit, S.A. Jonker, J.W. Verhoeven, H. Oevering, J. Kroon, M.N. Paddon-Row, A.M. Oliver, Chem. Phys. 170 (1993) 359.
[80] S.I. Khan, A.M. Oliver, M.N. Paddon-Row, Y. Rubin, J. Am. Chem. Soc. 115 (1993) 4919.
[81] S. Larsson, A. Volosov, J. Chem. Phys. 85 (1986) 2548.
[82] S. Larsson, A. Volosov, J. Chem. Phys. 87 (1987) 6623.
[83] S. Larsson, Chem. Scr. 28A (1988) 15.
[84] A.W. Axup, M. Albin, S.L. Mayo, R.J. Crutchley, H.B. Gray, J. Am. Chem. Soc. 110 (1988) 435.
[85] M.J. Therien, J. Chang, A.L. Raphael, B.E. Bowler, H.B. Gray, Struct. Bond. 75 (1991) 109.
[86] D.R. Casimiro, L.L. Wong, J.L. Colon, T.E. Zewert, J.H. Richards, I.J. Chang, J.R. Winkler, H.B. Gray, J. Am. Chem. Soc. 115 (1993) 1485.
[87] M.J. Bjerrum, D.R. Casimiro, I.J. Chang, A.J. Dibilio, H.B. Gray, M.G. Hill, R. Langen, G.A. Mines, L.K. Skov, J.R. Winkler, D.S. Wuttke, J. Bioenerg. Biomembr. 27 (1995) 295.
[88] R. Langen, J.L. Colon, D.R. Casimiro, T.B. Karpishin, J.R. Winkler, H.B. Gray, J. Biol. Inorg. Chem. 1 (1996) 221.
[89] J.R. Winkler, H.B. Gray, J. Biol. Inorg. Chem. 2 (1997) 399.
[90] S.S. Isied, A. Vassilian, J.F. Wishart, C. Creutz, H.A. Schwarz, N. Sutin, J. Am. Chem. Soc. 110 (1988) 635.
[91] M.D. Purugganan, C.V. Kumar, N.J. Turro, J.K. Barton, Science 241 (1988) 1645.
[92] C.J. Murphy, M.R. Arkin, Y. Jenkins, N.D. Ghatlia, S.H. Bossmann, N.J. Turro, J.K. Barton, Science 262 (1993) 1025.
[93] M.R. Arkin, E.D.A. Stemp, R.E. Holmlin, J.K. Barton, A. Hormann, E.J.C. Olson, P.F. Barbara, Science 273 (1996) 475.
[94] D.B. Hall, R.E. Holmlin, J.K. Barton, Nature 382 (1996) 731.
[95] S.O. Kelley, J.K. Barton, Science 283 (1999) 375.
[96] M.E. Nunez, D.B. Hall, J.K. Barton, Chem. Biol. 6 (1999) 85.
[97] C.Z. Wan, T. Fiebig, S.O. Kelley, C.R. Treadway, J.K. Barton, A.H. Zewail, Proc. Natl. Acad. Sci. U. S. A. 96 (1999) 6014.
[98] S.O. Kelley, N.M. Jackson, M.G. Hill, J.K. Barton, Angew. Chem. Int. Ed. 38 (1999) 941.
[99] C.Z. Wan, T. Fiebig, O. Schiemann, J.K. Barton, A.H. Zewail, Proc. Natl. Acad. Sci. U. S. A. 97 (2000) 14052.
[100] P.K. Bhattacharya, J.K. Barton, J. Am. Chem. Soc. 123 (2001) 8649.
[101] C.R. Treadway, M.G. Hill, J.K. Barton, Chem. Phys. 281 (2002) 409.
[102] M. Pascaly, J. Yoo, J.K. Barton, J. Am. Chem. Soc. 124 (2002) 9083.
[103] M.A. O'Neill, J.K. Barton, J. Am. Chem. Soc. 124 (2002) 13053.
[104] M.A. O'Neill, J.K. Barton, Proc. Natl. Acad. Sci. U. S. A. 99 (2002) 16543.
[105] S. Delaney, J.K. Barton, J. Org. Chem. 68 (2003) 6475.
[106] T.T. Williams, C. Dohno, E.D.A. Stemp, J.K. Barton, J. Am. Chem. Soc. 126 (2004) 8148.
[107] M.A. O'Neill, J.K. Barton, J. Am. Chem. Soc. 126 (2004) 11471.
[108] F.W. Shao, M.A. O'Neill, J.K. Barton, Proc. Natl. Acad. Sci. U. S. A. 101 (2004) 17914.
[109] F.W. Shao, K. Augustyn, J.K. Barton, J. Am. Chem. Soc. 127 (2005) 17445.
[110] X.F. Guo, A.A. Gorodetsky, J. Hone, J.K. Barton, C. Nuckolls, Nat. Nanotechnol. 3 (2008) 163.
[111] J.C. Genereux, K.E. Augustyn, M.L. Davis, F.W. Shao, J.K. Barton, J. Am. Chem. Soc. 130 (2008) 15150.
[112] M.Y. Ogawa, I. Moreira, J.F. Wishart, S.S. Isied, Chem. Phys. 176 (1993) 589.
[113] M.Y. Ogawa, J.F. Wishart, Z.Y. Young, J.R. Miller, S.S. Isied, J. Phys. Chem. 97 (1993) 11456.
[114] Y.G.K. Shin, M.D. Newton, S.S. Isied, J. Am. Chem. Soc. 125 (2003) 3722.
[115] R.A. Malak, Z.N. Gao, J.F. Wishart, S.S. Isied, J. Am. Chem. Soc. 126 (2004) 13888.
[116] M.D. Johnson, J.R. Miller, N.S. Green, G.L. Closs, J. Phys. Chem. 93 (1989) 1173.
[117] L.A. Curtiss, C.A. Naleway, J.R. Miller, Chem. Phys. 176 (1993) 387.
[118] L.A. Curtiss, C.A. Naleway, J.R. Miller, J. Phys. Chem. 99 (1995) 1182.
[119] L.A. Curtiss, J.R. Miller, J. Phys. Chem. A 102 (1998) 160.
[120] B. Paulson, K. Pramod, P. Eaton, G. Closs, J.R. Miller, J. Phys. Chem. 97 (1993) 13042.
[121] B.P. Paulson, L.A. Curtiss, B. Bal, G.L. Closs, J.R. Miller, J. Am. Chem. Soc. 118 (1996) 378.
[122] K.S. Schanze, L.A. Cabana, J. Phys. Chem. 94 (1990) 2740.
[123] D.N. Beratan, J.N. Betts, J.N. Onuchic, Science 252 (1991) 1285.
[124] S. Priyadarshy, S.M. Risser, D.N. Beratan, J. Phys. Chem. 100 (1996) 17678.
[125] I.V. Kurnikov, G.S.M. Tong, M. Madrid, D.N. Beratan, J. Phys. Chem. B 106 (2002) 7.
[126] G.S.M. Tong, I.V. Kurnikov, D.N. Beratan, J. Phys. Chem. B 106 (2002) 2381.
[127] J. Zheng, Y.K. Kang, M.J. Therien, D.N. Beratan, J. Am. Chem. Soc. 127 (2005) 11303.
[128] S.S. Skourtis, I.A. Balabin, T. Kawatsu, D.N. Beratan, Proc. Natl. Acad. Sci. U. S. A. 102 (2005) 3552.
[129] D.N. Beratan, S.S. Skourtis, I.A. Balabin, A. Balaeff, S. Keinan, R. Venkatramani, D.Q. Xiao, Acc. Chem. Res. 42 (2009) 1669.
[130] A. Osuka, T. Nagata, K. Maruyama, N. Mataga, T. Asahi, I. Yamazaki, Y. Nishimura, Chem. Phys. Lett. 185 (1991) 88.
[131] A. Osuka, S. Nakajima, K. Maruyama, N. Mataga, T. Asahi, I. Yamazaki, Y. Nishimura, T. Ohno, K. Nozaki, J. Am. Chem. Soc. 115 (1993) 4577.
[132] T. Asahi, M. Ohkohchi, R. Matsusaka, N. Mataga, R.P. Zhang, A. Osuka, K. Maruyama, J. Am. Chem. Soc. 115 (1993) 5665.
[133] A.M. Brun, A. Harriman, J. Am. Chem. Soc. 114 (1992) 3656.
[134] A. Harriman, F. Odobel, J.P. Sauvage, J. Am. Chem. Soc. 117 (1995) 9461.
[135] A. Harriman, Angew. Chem. Int. Ed. 38 (1999) 945.
[136] A. Harriman, A. Khatyr, R. Ziessel, A.C. Benniston, Angew. Chem. Int. Ed. 39 (2000) 4287.
[137] A. Harriman, L.J. Mallon, K.J. Elliot, A. Haefele, G. Ulrich, R. Ziessel, J. Am. Chem. Soc. 131 (2009) 13375.
[138] O. Farver, I. Pecht, J. Am. Chem. Soc. 114 (1992) 5764.
[139] H. Heitele, F. Pollinger, K. Kremer, M.E. Michel-Beyerle, M. Futscher, G. Voit, J. Weiser, H.A. Staab, Chem. Phys. Lett. 188 (1992) 270.
[140] D.N. Blauch, J.M. Saveant, J. Phys. Chem. 97 (1993) 6444.
[141] S. Franzen, R.F. Goldstein, S.G. Boxer, J. Phys. Chem. 97 (1993) 3040.
[142] F. Barigelletti, L. Flamigni, V. Balzani, J.P. Collin, J.P. Sauvage, A. Sour, E.C. Constable, A. Thompson, J. Am. Chem. Soc. 116 (1994) 7692.
[143] F. Barigelletti, L. Flamigni, M. Guardigli, A. Juris, M. Beley, S. Chodorowski-Kimmes, J.P. Collin, J.P. Sauvage, Inorg. Chem. 35 (1996) 136.
[144] A.K. Mishra, R. Chandrasekar, M. Faraggi, M.H. Klapper, J. Am. Chem. Soc. 116 (1994) 1414.
[145] E.H. Yonemoto, R.L. Riley, Y.I. Kim, S.J. Atherton, R.H. Schmehl, T.E. Mallouk, J. Am. Chem. Soc. 114 (1992) 8081.
[146] E.H. Yonemoto, G.B. Saupe, R.H. Schmehl, S.M. Hubig, R.L. Riley, B.L. Iverson, T.E. Mallouk, J. Am. Chem. Soc. 116 (1994) 4786.
[147] M.T. Carter, G.K. Rowe, J.N. Richardson, L.M. Tender, R.H. Terrill, R.W. Murray, J. Am. Chem. Soc. 117 (1995) 2896.
[148] P.J.F. de Rege, S.A. Williams, M.J. Therien, Science 269 (1995) 1409.
[149] Y.K. Kang, I.V. Rubtsov, P.M. Iovine, J. Chen, M.J. Therien, J. Am. Chem. Soc. 124 (2002) 8275.
[150] N.P. Redmore, I.V. Rubtsov, M.J. Therien, J. Am. Chem. Soc. 125 (2003) 8769.
[151] I.V. Rubtsov, Y.K. Kang, N.P. Redmore, R.M. Allen, J. Zheng, D.N. Beratan, M.J. Therien, J. Am. Chem. Soc. 126 (2004) 5022.
[152] Y.K. Kang, T.V. Duncan, M.J. Therien, J. Phys. Chem. B 111 (2007) 6829.
[153] Y. Xing, T.H. Park, R. Venkatramani, S. Keinan, D.N. Beratan, M.J. Therien, E. Borguet, J. Am. Chem. Soc. 132 (2010) 7946.
[154] A.K. Felts, W.T. Pollard, R.A. Friesner, J. Phys. Chem. 99 (1995) 2929.
[155] C.E.D. Chidsey, Science 251 (1991) 919.
[156] J.F. Smalley, S.W. Feldberg, C.E.D. Chidsey, M.R. Linford, M.D. Newton, Y.P. Liu, J. Phys. Chem. 99 (1995) 13141.
[157] S.B. Sachs, S.P. Dudek, R.P. Hsung, L.R. Sita, J.F. Smalley, M.D. Newton, S.W. Feldberg, C.E.D. Chidsey, J. Am. Chem. Soc. 119 (1997) 10563.
[158] H.D. Sikes, J.F. Smalley, S.P. Dudek, A.R. Cook, M.D. Newton, C.E.D. Chidsey, S.W. Feldberg, Science 291 (2001) 1519.
[159] J. Cheng, D.B. Robinson, R.L. Cicero, T. Eberspacher, C.J. Barrelet, C.E.D. Chidsey, J. Phys. Chem. B 105 (2001) 10900.
[160] J.F. Smalley, H.O. Finklea, C.E.D. Chidsey, M.R. Linford, S.E. Creager, J.P. Ferraris, K. Chalfant, T. Zawodzinsk, S.W. Feldberg, M.D. Newton, J. Am. Chem. Soc. 125 (2003) 2004.
[161] J.F. Smalley, S.B. Sachs, C.E.D. Chidsey, S.P. Dudek, H.D. Sikes, S.E. Creager, C.J. Yu, S.W. Feldberg, M.D. Newton, J. Am. Chem. Soc. 126 (2004) 14620.
[162] G.L. Gaines, M.P. Oneil, W.A. Svec, M.P. Niemczyk, M.R. Wasielewski, J. Am. Chem. Soc. 113 (1991) 719.
[163] D.G. Johnson, M.P. Niemczyk, D.W. Minsek, G.P. Wiederrecht, W.A. Svec, G.L. Gaines, M.R. Wasielewski, J. Am. Chem. Soc. 115 (1993) 5692.
[164] W.B. Davis, W.A. Svec, M.A. Ratner, M.R. Wasielewski, Nature 396 (1998) 60.
[165] D. Segal, A. Nitzan, W.B. Davis, M.R. Wasielewski, M.A. Ratner, J. Phys. Chem. B 104 (2000) 3817.
[166] Y. Sakata, H. Tsue, M.P. Oneil, G.P. Wiederrecht, M.R. Wasielewski, J. Am. Chem. Soc. 116 (1994) 6904.
[167] W.B. Davis, M.A. Ratner, M.R. Wasielewski, J. Am. Chem. Soc. 123 (2001) 7877.
[168] E.A. Weiss, M.J. Ahrens, L.E. Sinks, A.V. Gusev, M.A. Ratner, M.R. Wasielewski, J. Am. Chem. Soc. 126 (2004) 5577.
[169] R.H. Goldsmith, L.E. Sinks, R.F. Kelley, L.J. Betzen, W.H. Liu, E.A. Weiss, M.A. Ratner, M.R. Wasielewski, Proc. Natl. Acad. Sci. U. S. A. 102 (2005) 3540.
[170] R.H. Goldsmith, O. DeLeon, T.M. Wilson, D. Finkelstein-Shapiro, M.A. Ratner, M.R. Wasielewski, J. Phys. Chem. A 112 (2008) 4410.
[171] R.F. Kelley, S.J. Lee, T.M. Wilson, Y. Nakamura, D.M. Tiede, A. Suka, J.T. Hupp, M.R. Wasielewski, J. Am. Chem. Soc. 130 (2008) 4277.
[172] G.B. Schuster, X.Q. Yang, C.F. Zou, B. Sauerwein, J. Photochem. Phtobiol. A 65 (1992) 191.
[173] D. Ly, L. Sanii, G.B. Schuster, J. Am. Chem. Soc. 121 (1999) 9400.
[174] L. Sanii, G.B. Schuster, J. Am. Chem. Soc. 122 (2000) 11545.
[175] C.S. Liu, R. Hernandez, G.B. Schuster, J. Am. Chem. Soc. 126 (2004) 2877.
[176] G.B. Schuster, U. Landman, in: G.B. Schuster (Ed.), Long-range Charge Transfer in DNA I, 2004, p. 139.
[177] S.M. Risser, D.N. Beratan, T.J. Meade, J. Am. Chem. Soc. 115 (1993) 2508.
[178] T.J. Meade, J.F. Kayyem, Angew. Chem. Int. Ed. Engl. 34 (1995) 352.
[179] E.S. Krider, T.J. Meade, J. Biol. Inorg. Chem. 3 (1998) 222.
[180] F.D. Lewis, T.F. Wu, Y.F. Zhang, R.L. Letsinger, S.R. Greenfield, M.R. Wasielewski, Science 277 (1997) 673.
[181] F.D. Lewis, X.Y. Liu, J.Q. Liu, S.E. Miller, R.T. Hayes, M.R. Wasielewski, Nature 406 (2000) 51.
[182] F.D. Lewis, R.S. Kalgutkar, Y.S. Wu, X.Y. Liu, J.Q. Liu, R.T. Hayes, S.E. Miller, M.R. Wasielewski, J. Am. Chem. Soc. 122 (2000) 12346.

[183] F.D. Lewis, X.Y. Liu, S.E. Miller, R.T. Hayes, M.R. Wasielewski, J. Am. Chem. Soc. 124 (2002) 11280.
[184] F.D. Lewis, J.Q. Liu, X.B. Zuo, R.T. Hayes, M.R. Wasielewski, J. Am. Chem. Soc. 125 (2003) 4850.
[185] F.D. Lewis, Y.S. Wu, L.G. Zhang, X.B. Zuo, R.T. Hayes, M.R. Wasielewski, J. Am. Chem. Soc. 126 (2004) 8206.
[186] F.D. Lewis, M.R. Wasielewski, in: G.B. Schuster (Ed.), Long-range Charge Transfer in DNA I, 2004, p. 45.
[187] J. Vura-Weis, M.R. Wasielewski, A.K. Thazhathveetil, F.D. Lewis, J. Am. Chem. Soc. 131 (2009) 9722.
[188] F.D. Lewis, A.K. Thazhathveetil, T.A. Zeidan, J. Vura-Weis, M.R. Wasielewski, J. Am. Chem. Soc. 132 (2010) 444.
[189] K. Fukui, K. Tanaka, Angew. Chem. Int. Ed. 37 (1998) 158.
[190] K. Fukui, K. Tanaka, M. Fujitsuka, A. Watanabe, O. Ito, J. Photochem. Photobiol. B 50 (1999) 18.
[191] K. Fukui, Electrochemistry 68 (2000) 992.
[192] E. Meggers, M.E. Michel-Beyerle, B. Giese, J. Am. Chem. Soc. 120 (1998) 12950.
[193] B. Giese, S. Wessely, M. Spormann, U. Lindemann, E. Meggers, M.E. Michel-Beyerle, Angew. Chem. Int. Ed. 38 (1999) 996.
[194] E. Meggers, A. Dussy, T. Schafer, B. Giese, Chem. Eur. J. 6 (2000) 485.
[195] B. Giese, J. Amaudrut, A.K. Kohler, M. Spormann, S. Wessely, Nature 412 (2001) 318.
[196] B. Giese, A. Biland, Chem. Commun. (2002) 667.
[197] B. Giese, B. Carl, T. Carl, T. Carell, C. Behrens, U. Hennecke, O. Schiemann, E. Feresin, Angew. Chem. Int. Ed. 43 (2004) 1848.
[198] M. Bixon, B. Giese, S. Wessely, T. Langenbacher, M.E. Michel-Beyerle, J. Jortner, Proc. Natl. Acad. Sci. U. S. A. 96 (1999) 11713.
[199] M. Bixon, J. Jortner, J. Phys. Chem. B 104 (2000) 3906.
[200] M. Bixon, J. Jortner, J. Am. Chem. Soc. 123 (2001) 12556.
[201] M. Bixon, J. Jortner, Chem. Phys. 281 (2002) 393.
[202] M. Bixon, J. Jortner, Russ. J. Electrochem. 39 (2003) 3.
[203] M. Bixon, J. Jortner, Chem. Phys. 319 (2005) 273.
[204] J. Jortner, M. Bixon, J. Chem. Phys. 88 (1988) 167.
[205] J. Jortner, M. Bixon, B. Wegewijs, J.W. Verhoeven, R.P.H. Rettschnick, Chem. Phys. Lett. 205 (1993) 451.
[206] J. Jortner, M. Bixon, T. Langenbacher, M.E. Michel-Beyerle, Proc. Natl. Acad. Sci. U. S. A. 95 (1998) 12759.
[207] J. Jortner, M. Bixon, A.A. Voityuk, N. Rosch, J. Phys. Chem. A 106 (2002) 7599.
[208] A.A. Voityuk, N. Rosch, M. Bixon, J. Jortner, J. Phys. Chem. B 104 (2000) 9740.
[209] A.A. Voityuk, J. Jortner, M. Bixon, N. Rosch, J. Chem. Phys. 114 (2001) 5614.
[210] A.A. Voityuk, N. Rosch, J. Phys. Chem. B 106 (2002) 3013.
[211] A.A. Voityuk, W.B. Davis, J. Phys. Chem. B 111 (2007) 2976.
[212] A.A. Voityuk, J. Phys. Chem. C 111 (2007) 7207.
[213] H. Imahori, K. Tamaki, D.M. Guldi, C.P. Luo, M. Fujitsuka, O. Ito, Y. Sakata, S. Fukuzumi, J. Am. Chem. Soc. 123 (2001) 2607.
[214] H. Imahori, Y. Sekiguchi, Y. Kashiwagi, T. Sato, Y. Araki, O. Ito, H. Yamada, S. Fukuzumi, Chem. Eur. J. 10 (2004) 3184.
[215] R. Rathore, S.H. Abdelwahed, M.K. Kiesewetter, R.C. Reiter, C.D. Stevenson, J. Phys. Chem. B 110 (2006) 1536.
[216] Y.A. Berlin, A.L. Burin, M.A. Ratner, J. Am. Chem. Soc. 123 (2001) 260.
[217] Y.A. Berlin, A.L. Burin, M.A. Ratner, J. Phys. Chem. A 104 (2000) 443.
[218] Y.A. Berlin, A.L. Burin, M.A. Ratner, Chem. Phys. 275 (2002) 61.
[219] F.C. Grozema, L.D.A. Siebbeles, Y.A. Berlin, M.A. Ratner, ChemPhysChem 3 (2002) 536.
[220] Y.A. Berlin, I.V. Kurnikov, D. Beratan, M.A. Ratner, A.L. Burin, Top. Curr. Chem. 237 (2004) 1.
[221] L.D. Sparks, W.R. Scheidt, J.A. Shelnutt, Inorg. Chem. 31 (1992) 2191.
[222] H.A. Staab, J. Weiser, E. Baumann, Chem. Ber. Recl. 125 (1992) 2275.
[223] H.A. Staab, J. Weiser, M. Futscher, G. Voit, A. Ruckemann, C. Anders, Chem. Ber. Recl. 125 (1992) 2285.
[224] H.A. Staab, G. Voit, J. Weiser, M. Futscher, Chem. Ber. Recl. 125 (1992) 2303.
[225] C. Krieger, M. Dernbach, G. Voit, T. Carell, H.A. Staab, Chem. Ber. Recl. 126 (1993) 811.
[226] H. Heitele, F. Pollinger, T. Haberle, M.E. Michel-Beyerle, H.A. Staab, J. Phys. Chem. 98 (1994) 7402.
[227] H.A. Staab, C. Krieger, C. Anders, A. Ruckemann, Chem. Ber. 127 (1994) 231.
[228] H.A. Staab, A. Feurer, R. Hauck, Angew. Chem. Int. Ed. 33 (1994) 2428.
[229] H.A. Staab, A. Feurer, C. Krieger, A.S. Kumar, Liebigs Ann. Recl. (1997) 2321.
[230] H.A. Staab, B. Kratzer, S. Quazzotti, Eur. J. Org. Chem. (1998) 2149.
[231] H.A. Staab, R. Hauck, B. Popp, Eur. J. Org. Chem. (1998) 631.
[232] A.R. Wartini, J. Valenzuela, H.A. Staab, F.A. Neugebauer, Eur. J. Org. Chem. (1998) 221.
[233] A.R. Wartini, J. Valenzuela, H.A. Staab, F.A. Neugebauer, Eur. J. Org. Chem. (1998) 139.
[234] R. Rathore, S.H. Abdelwahed, I.A. Guzei, J. Am. Chem. Soc. 125 (2003) 8712.
[235] R. Rathore, V.J. Chebny, E.J. Kopatz, I.A. Guzei, Angew. Chem. Int. Ed. 44 (2005) 2771.
[236] A.M. Napper, I. Read, D.H. Waldeck, N.J. Head, A.M. Oliver, M.N. Paddon-Row, J. Am. Chem. Soc. 122 (2000) 5220.
[237] A.M. Napper, H.Y. Liu, D.H. Waldeck, J. Phys. Chem. B 105 (2001) 7699.
[238] A.M. Napper, N.J. Head, A.M. Oliver, M.J. Shephard, M.N. Paddon-Row, I. Read, D.H. Waldeck, J. Am. Chem. Soc. 124 (2002) 10171.
[239] A.M. Napper, I. Read, R. Kaplan, M.B. Zimmt, D.H. Waldeck, J. Phys. Chem. A 106 (2002) 5288.
[240] F.D. Lewis, P. Daublain, G.B. Delos Santos, W.Z. Liu, A.M. Asatryan, S.A. Markarian, T. Fiebig, M. Raytchev, Q.A. Wang, J. Am. Chem. Soc. 128 (2006) 4792.
[241] T.A. Zeidan, Q. Wang, T. Fiebig, F.D. Lewis, J. Am. Chem. Soc. 129 (2007) 9848.
[242] C.A. Hunter, J.K.M. Sanders, J. Am. Chem. Soc. 112 (1990) 5525.
[243] C.A. Hunter, Angew. Chem. Int. Ed. Engl. 32 (1993) 1584.
[244] D.A. Dougherty, Science 271 (1996) 163.
[245] P.M. Iovine, M.A. Kellett, N.P. Redmore, M.J. Therien, J. Am. Chem. Soc. 122 (2000) 8717.
[246] P.M. Iovine, G. Veglia, G. Furst, M.J. Therien, J. Am. Chem. Soc. 123 (2001) 5668.
[247] H.O. House, D.G. Koepsell, W.J. Campbell, J. Org. Chem. 37 (1972) 1003.
[248] R.L. Clough, W.J. Kung, R.E. Marsh, J.D. Roberts, J. Org. Chem. 41 (1976) 3603.
[249] J. Fajer, D.C. Borg, A. Forman, D. Dolphin, R.H. Felton, J. Am. Chem. Soc. 92 (1970) 3451.
[250] L. Reynolds, J.A. Gardecki, S.J.V. Frankland, M.L. Horng, M. Maroncelli, J. Phys. Chem. 100 (1996) 10337.
[251] F.D. Lewis, X. Liu, S.E. Miller, M.R. Wasielewski, J. Am. Chem. Soc. 121 (1999) 9746.
[252] A. Osuka, K. Maruyama, N. Mataga, T. Asahi, I. Yamazaki, N. Tamai, J. Am. Chem. Soc. 112 (1990) 4958.
[253] T. Kato, M. Tachiya, Chem. Phys. Lett. 241 (1995) 463.
[254] X. Amashukeli, N.E. Gruhn, D.L. Lichtenberger, J.R. Winkler, H.B. Gray, J. Am. Chem. Soc. 126 (2004) 15566.
[255] M.J.E.A. Frisch, Gaussian 03, Revision C.02, Gaussian, Inc., Wallingford, CT, 2004.
[256] N. Liang, J.R. Miller, G.L. Closs, J. Am. Chem. Soc. 111 (1989) 8740.
[257] N. Liang, J.R. Miller, G.L. Closs, J. Am. Chem. Soc. 112 (1990) 5353.
[258] R.C. Reid, J.M. Prausnitz, B.R. Poling, The Properties of Gases and Liquids, 4th ed., McGraw-Hill Companies, 1987.
[259] L.R. Khundkar, J.W. Perry, J.E. Hanson, P.B. Dervan, J. Am. Chem. Soc. 116 (1994) 9700.
[260] K. Shinsaka, N. Gee, G.R. Freeman, J. Chem. Thermodyn. 17 (1985) 1111.
[261] P. Finckh, H. Heitele, M. Volk, M.E. Michel-Beyerle, J. Phys. Chem. 92 (1988) 6584.
[262] J.K. Delaney, D.C. Mauzerall, J.S. Lindsey, J. Am. Chem. Soc. 112 (1990) 957.
[263] P.Y. Chen, S.L. Mecklenburg, T.J. Meyer, J. Phys. Chem. 97 (1993) 13126.
[264] M. Maroncelli, J. Macinnis, G.R. Fleming, Science 243 (1989) 1674.
[265] E.M. Kosower, D. Huppert, Chem. Phys. Lett. 96 (1983) 433.
[266] M. McGuire, G. McLendon, J. Phys. Chem. 90 (1986) 2549.
[267] H. Heitele, M.E. Michel-Beyerle, P. Finckh, Chem. Phys. Lett. 138 (1987) 237.
[268] J.D. Simon, S.G. Su, J. Phys. Chem. 92 (1988) 2395.
[269] T.J. Kang, M.A. Kahlow, D. Giser, S. Swallen, V. Nagarajan, W. Jarzeba, P.F. Barbara, J. Phys. Chem. 92 (1988) 6800.
[270] L.D. Zusman, Chem. Phys. 49 (1980) 295.
[271] D.F. Calef, P.G. Wolynes, J. Phys. Chem. 87 (1983) 3387.
[272] D.F. Calef, P.G. Wolynes, J. Chem. Phys. 78 (1983) 470.
[273] A. Garg, J.N. Onuchic, V. Ambegaokar, J. Chem. Phys. 83 (1985) 4491.
[274] J.N. Onuchic, J. Chem. Phys. 86 (1987) 3925.
[275] J.T. Hynes, J. Phys. Chem. 90 (1986) 3701.
[276] I. Rips, J. Jortner, J. Chem. Phys. 87 (1987) 2090.
[277] I. Rips, J. Jortner, J. Chem. Phys. 87 (1987) 6513.
[278] I. Rips, J. Jortner, Chem. Phys. Lett. 133 (1987) 411.
[279] M. Sparpaglione, S. Mukamel, J. Phys. Chem. 91 (1987) 3938.
[280] M. Sparpaglione, S. Mukamel, J. Chem. Phys. 88 (1988) 3263.
[281] M. Sparpaglione, S. Mukamel, J. Chem. Phys. 88 (1988) 1465.
[282] G.E. McManis, A. Gochev, M.J. Weaver, Chem. Phys. 152 (1991) 107.
[283] M. Morillo, R.I. Cukier, J. Chem. Phys. 89 (1988) 6736.
[284] A. Masad, D. Huppert, E.M. Kosower, Chem. Phys. 144 (1990) 391.
[285] G.P. Wiederrecht, W.A. Svec, M.R. Wasielewski, J. Phys. Chem. B 103 (1999) 1386.
[286] L.E. Sinks, M.R. Wasielewski, J. Phys. Chem. A 107 (2003) 611.
[287] M. Liu, N. Ito, M. Maroncelli, D.H. Waldeck, A.M. Oliver, M.N. Paddon-Row, J. Am. Chem. Soc. 127 (2005) 17867.
[288] D.W. Davidson, R.H. Cole, J. Chem. Phys. 18 (1950) 1417.
[289] D.W. Davidson, R.H. Cole, J. Chem. Phys. 19 (1951).
[290] Michele-Beyerle observed $\gamma \sim 0.5$ in Ref. [267].
[291] D. Devault, B. Chance, Biophys. J. 6 (1966) 825.
[292] H.S. Eom, S.C. Jeoung, D. Kim, J.-H. Ha, Y.-R. Kim, J. Phys. Chem. A 101 (1997) 3661.
[293] G.G. Gurzadyan, T.H. Tran-Thi, T. Gustavsson, J. Chem. Phys. 108 (1998) 385.
[294] S. Akimoto, T. Yamazaki, I. Yamazaki, A. Osuka, Chem. Phys. Lett. 309 (1999) 177.
[295] N. Mataga, Y. Shibata, H. Chosrowjan, N. Yoshida, A. Osuka, J. Phys. Chem. B 104 (2000) 4001.
[296] H.-Z. Yu, J.S. Baskin, A.H. Zewail, J. Phys. Chem. A 106 (2002) 9845.
[297] N.W. Song, H.S. Cho, M.-C. Yoon, S.C. Jeoung, N. Yoshida, A. Osuka, D. Kim, Bull. Chem. Soc. Jpn. 75 (2002) 1023.
[298] S. Engleitner, M. Seel, W. Zinth, J. Phys. Chem. A 103 (1999) 3013.
[299] J.E. Moser, M. Wolf, F. Lenzmann, M. Gratzel, Z. Phys. Chem. 212 (1999) 85.
[300] F. Lenzmann, J. Krueger, S. Burnside, K. Brooks, M. Gratzel, D. Gal, S. Ruhle, D. Cahen, J. Phys. Chem. B 105 (2001) 6347.
[301] C. Zimmermann, F. Willig, S. Ramakrishna, B. Burfeindt, B. Pettinger, R. Eichberger, W. Storck, J. Phys. Chem. B 105 (2001) 9245.
[302] L.E. Shaw, C.H. Langford, Coord. Chem. Rev. 230 (2002) 165.
[303] J. Kallioinen, G. Benko, V. Sundstrom, J.E.I. Korppi-Tommola, A.P. Yartsev, J. Phys. Chem. B 106 (2002) 4396.
[304] C. Wan, T. Xia, H.-C. Becker, A.H. Zewail, Chem. Phys. Lett. 412 (2005) 158.

[305] R.S. Mulliken, J. Am. Chem. Soc. 74 (1952) 811.
[306] N.S. Hush, Prog. Inorg. Chem. 8 (1967) 391.
[307] N. Sutin, Electron Transfer-from Isolated Molecules to Biomolecules Pt 1, vol. 106, 1999, p. 7.
[308] I.V. Rubtsov, Y.K. Kang, M.J. Therien, unpublished results.
[309] R.J. Cave, M.D. Newton, Chem. Phys. Lett. 249 (1996) 15.
[310] R.J. Cave, M.D. Newton, J. Chem. Phys. 106 (1997) 9213.
[311] J.R. Reimers, N.S. Hush, J. Phys. Chem. 95 (1991) 9773.
[312] M. Rust, J. Lappe, R.J. Cave, J. Phys. Chem. A 106 (2002) 3930.
[313] M.C. Zerner, G.H. Loew, R.F. Kirchner, U.T. Muellerwesterhoff, J. Am. Chem. Soc. 102 (1980) 589.
[314] M.A.M.A.C. Thompson, W. ArgusLab 4.0; Planaria Software LLC, Seattle, 2004, http://www.arguslab.com.
[315] Note that the tabulated D–A distances for the PM3-based (**2**–**3**)**a-Zn** structures are smaller than those for the DFT-based structures. This derives from the fact that the axis through the centers of the phenyl and quinonyl rings is not perpendicular to the porphyrin plane, not because of tighter stacking between the rings.